REAL TIME TEMPERATURE MEASUREMENT USING GRADIENT ECHO MAGNETIC RESONANCE IMAGING

by

Volkan Büyükgüngör

B.S. in Electrical and Electronic Engineering, Boğaziçi University, 2004

Submitted to the Institute of Biomedical Engineering
in partial fulfillment of the requirements
for the degree of
Master of Science
in
Biomedical Engineering

Boğaziçi University
May 2008

REAL TIME TEMPERATURE MEASUREMENT USING GRADIENT ECHO MAGNETIC RESONANCE IMAGING

APPROVED BY:

Doç. Dr. Cengizhan Öztürk
(Thesis Advisor)

Yrd. Doç. Dr. Ata Akın
(Thesis Co-advisor)

Doç. Dr. Kubilay Aydın
(Thesis Co-advisor)

DATE OF APPROVAL: 06.06.2008

ACKNOWLEDGMENTS

I would like to thank my thesis supervisor Assoc. Prof. Dr. Cengizhan Öztürk for introducing me to MRI, providing a spectacular working environment, his bottomless support, and above all for being who he is.

I would also like to thank my committee members Assoc. Prof. Dr. Kubilay Aydın and Assist. Prof. Dr. Ata Akın for their suggestions and evaluations.

I would like to mention Uzay Emrah Emir, his valuable discussions and helpful insights.

Finally, I would like to thank my family for supporting me throughout this thesis in every way possible.

ABSTRACT

REAL TIME TEMPERATURE MEASUREMENT USING GRADIENT ECHO MAGNETIC RESONANCE IMAGING

Heat induced local therapies play a significant role in several medical procedures, a major field being tumor ablation. Regardless of the temperature range and the heat application method of these different hyperthermia applications, they all require the solution of the following problem: Determination of spatial and temporal distribution of temperature (thus the effects and side effects of treatment) within the applied region. A targeted temperature monitoring system with sufficient capabilities would enable focusing, localization, thermal dose planning, collateral damage prevention and validation of treatment. First four of the above inherently need to be interactive, thus require real time monitoring. For a real-time application, underlying goal is to provide a relative or absolute temperature measurement, fast enough to use the temperature data to intervene with the medical procedure. MRTI (Magnetic Resonance Temperature Imaging) with PRF shift method is first proposed as a way to provide fast temperature maps during thermal therapies by Ishihara in 1992. It provides a way to use the phase images from GRE sequences to extract temperature difference information between successive acquisitions. In this thesis, an attempt is made to implement all parts of an MR-based temperature measurement system, which consists of an appropriate GRE sequence, post processing, and visualization code. The system will have the potential of being adapted to an MRI console in order to create an interactive real-time temperature monitoring application.

Keywords: Invivo Temperature Mapping, Magnetic Resonance Imaging, MRTI (MR Temperature Imaging)

ÖZET

MANYETİK RESONANS GÖRÜNTÜLEME KULLANARAK GERÇEK ZAMANLI SICAKLIK ÖLÇÜMÜ

Isıl lokal terapiler tümör yakma başta olmak üzere birçok tıbbi müdahalede önemli rol oynar. Bu tür tedavilerde, uygulanan sıcaklık aralığından ve yönteminden bağımsız olarak aşağıdaki sorunun giderilmesi gerekir: Müdahalenin etkileri ve yan etkileri belirlenebilecek şekilde, sıcaklığın uygulanan bölgedeki uzaysal ve zamansal dağılımının tayin edilmesi. İdeal bir sıcaklık izleme sistemi odaklama, yerleştirme, ısıl doz ayarlama yapabilmeli, ikincil hasarı engelleyebilmeli, ve yapılan işlemi doğrulayabilmelidir. Bu yukarıdakilerin ilk dördü yapısı gereği interaktif erişim gerektirir. Bu da ancak gerçek zamanlı izleme ile mümkündür. Bu tür uygulamalarda, uygulanan tıbbi işleme gerektiğinde müdahale edebilecek kadar hızlı bilgi akışı sağlanabilinirse, izleme sistemi gerçek zamanlı kabul edilebilir. PRF (Proton Rezonans Frekansı) kayması yöntemi ile MRTI (Manyetik Rezonans Sıcaklık Görüntüleme) ilk kez 1992 yılında, ısıl tedaviler sırasında hızlı sıcaklık haritaları sağlamak amacıyla Ishihara tarafından önerilmiştir. Bu yöntem ardışık çekimler arasındaki sıcaklık farkı bilgisini, GRE sekansı ile oluşturulan faz imgelerinden çıkartmaya dayanır. Bu tezde, uygun bir GRE sekansı, görüntü işleme ve görüntüleme kod bloklarına sahip, MR-tabanlı bir sıcaklık izleme sistemi oluşturulmaya çalışılmıştır.

Anahtar sözcükler: Invivo Sıcaklık Haritalama, Manyetik Rezonans Görüntüleme, MR Termal Görüntüleme

TABLE OF CONTENTS

ACKNOWLEDGMENTS iii
ABSTRACT iv
ÖZET v
LIST OF FIGURES viii
LIST OF TABLES x
LIST OF SYMBOLS xi
LIST OF ABBREVIATIONS xii
1. INTRODUCTION 1
1.1 Motivation 1
1.2 Outline of the Thesis 3
2. BACKGROUND 5
2.1 Hyperthermia 5
2.1.1 Types of Hyperthermia 6
2.1.1.1 LITT (Laser Induced Thermotherapy) 6
2.1.1.2 FUS (Focused Ultrasound Surgery) 6
2.1.1.3 RFA (Radio Frequency Ablation) 7
2.1.1.4 Microwave Ablation 7
2.1.1.5 Cryoablation 7
2.2 Temperature Monitoring Systems 7
2.2.1 Temperature Imaging with CT 7
2.2.2 Temperature Imaging with US 8
2.2.3 MRTI (Magnetic Resonance Temperature Imaging) 8
2.3 Physics of MR Parameters 8
2.3.1 Longitudinal Relaxation Time (T_1) 9
2.3.2 Diffusion Coefficient (D) 10
2.3.3 Proton Resonance Frequency (PRF) 12
2.4 GRE (Gradient Recalled Echo Imaging) 16
2.5 Phase Drift 16
2.6 Further Studies on PRF Methods 18

2.7 High Frequency Focused Ultrasound (HIFU) 19
3. EXPERIMENTAL SETUP 21
3.1 Overview 21
3.2 Water Heating and Circulation 21
3.2.1 Materials 22
3.2.2 Description 23
3.3 Phantom 24
3.3.1 Gel Preperation 24
3.3.2 Phantom casings 27
3.4 Validation Experiments 31
3.4.1 General Validation 31
3.4.1.1 Results 32
3.4.1.2 Conclusion 34
3.4.2 Step Response 36
3.4.2.1 Results 36
3.4.2.2 Conclusion 38
4. PHASE DRIFT CORRECTION 41
4.1 Data and Analysis 41
4.2 Correction algorithm 42
5. TEMPERATURE MEASUREMENT WITH GRADIENT ECHO 46
6. EFFECT OF ECHO TIME ON THERMAL RESOLUTION 49
7. CONCLUSION 51
REFERENCES 53

LIST OF FIGURES

Figure 2.1	Temperature dependence of T1 values for different tissues	11
Figure 2.2	Temperature dependence of ADC (apparent diffusion coefficient) values for different tissues	12
Figure 2.3	Chemical shift of water vs. temperature	13
Figure 2.4	Timing diagram of a gradient recalled echo (GRE) sequence	17
Figure 2.5	A phase difference image with iso–phase contours	18
Figure 3.1	Simplified block diagram of hot water circulator	22
Figure 3.2	Outside appearance of the hot water circulator	23
Figure 3.3	Inside of the hot water circulator	24
Figure 3.4	Inside of the water tank	25
Figure 3.5	Rectangular Phantom. Picture and MR image	27
Figure 3.6	Tube of Agar gel to be used as reference	28
Figure 3.7	Tube of Agar gel to be heated during scan	28
Figure 3.8	Foam case for tube phantoms	29
Figure 3.9	Case with tube phantoms in place	29
Figure 3.10	Final look of the case and the tube phantoms. Picture and MR image	30
Figure 3.11	Setup diagram and location of temperature readings	32
Figure 3.12	Temperature vs. Time readings at various points of the setup	34
Figure 3.13	Setup diagram and location of temperature readings	37
Figure 3.14	Temperature vs. Time readings at various points of the setup	38
Figure 4.1	Rectangular gel phantom with heat insulation	41
Figure 4.2	Phase drift at constant room temperature	42
Figure 4.3	Region of analysis for phase drift correction	43
Figure 4.4	Regions of reference for phase drift correction	44
Figure 4.5	Effect of drift correction on measured temperature	45
Figure 5.1	Regions of reference for drift correction	46
Figure 5.2	Average Temperature vs. Time, over concentric circular regions.	47
Figure 5.3	Thermal Map snapshots during active heating	48

Figure 5.4	Thermal Map snapshots during cooling	48
Figure 6.1	Region of analysis for TE effect on thermal resolution	50
Figure 6.2	Mean variance of temperature difference measured at a single pixel vs. Echo time; under constant phantom temperature	50

LIST OF TABLES

Table 3.1	Calculated relaxation values of Agar gel with 3% Agar and $2mM$ $CuSO_4$	26
Table 3.2	Maximum rate of change obtained during heating with the setup	39
Table 3.3	Rate of change for passively cooling tube phantom	39

LIST OF SYMBOLS

α	Flip angle
α	Temperature dependence coefficient
B_0	Main magnetic field
B_1	RF magnetic field
θ	Phase angle
ϕ	Diameter
γ	Gyromagnetic Ratio
k	Boltzmann constant
T_1	Longitudinal relaxation time (spin-lattice relaxation time)
T_2	Transverse relaxation time (spin-spin relaxation time)
T_2^*	Longitudinal relaxation time including relaxations
TE	Echo Time
D	Diffusion coefficient

LIST OF ABBREVIATIONS

ADC	Apparent Diffusion Coefficient
CT	Computed Tomography
EM	Electromagnetic
FDA	Food and Drug Administration
FLASH	Fast Low Angle Single Shot
FUS	Focused Ultrasound
GRE	Gradient Echo
HIFU	High Frequency Focused Ultrasound
LHT	Local Hyperthermia
LITT	Laser Interstitial Thermal Therapy
MR	Magnetic Resonance
MRI	Magnetic Resonance Imaging
MRTI	Magnetic Resonance Temperature Imaging
PRF	Proton Resonance Frequency
RF	Radio Frequency
RFA	Radio Frequency Ablation
SNR	Signal to Noise Ratio
SE	Spin Echo
TE	Echo Time
TR	Repetition Time
TI	Inversion Time
US	Ultrasound

1. INTRODUCTION

1.1 Motivation

Heat induced local therapies play a significant role in several medical procedures, a major field being tumor ablation. Below are three main classes of hyperthermia applications, based on the means of heat application:

- Laser Induced Interstitial Therapy (LITT)
- Electromagnetic Hyperthermia (RF and Microwave)
- Focused Ultrasound Therapy (FUS), also known as High Frequency Focused Ultrasound (HIFU)

Regardless of the temperature range and the heat application method of these different hyperthermia applications, they all require the solution of the following problem: Determination of spatial and temporal distribution of temperature (thus the effects and side effects of treatment) within the applied region. Such a knowledge of temperature distribution will enable,

- Focusing,
- Localization,
- Thermal dose planning,
- Preventing damage to surroundings,
- Validation of treatment.

First four of the above inherently need to be interactive, thus require real time monitoring.

Up until now, different approaches have been used to handle the problem stated above. Some of them are:

- Modeling
- Invasive usage of thermistors
- CT monitoring
- US monitoring
- MR monitoring

Each method has its drawbacks. Modeling approaches can be extremely inaccurate due to simplifying assumptions of physical phenomena and lack of exact knowledge of tissue constructs and parameters. It is possible to obtain excellent temporal and thermal resolution with thermistors, but they provide the poorest spatial representation if at all, and invasive methods should be avoided whenever possible. Ultrasound imaging has penetration constraints and is a very weak modality in terms of structural imaging. CT scanning brings the issue of radiation exposure, proposed method is highly dependent on tissue type, and is not a particularly fast modality.

When compared to the others methods, MRTI (Magnetic Resonance Temperature Imaging) has a relatively short history. The idea is investigated since Ishihara's proposal in 1992, based on which the first article is published in 1994. His method was based on PRF (Proton Resonance Frequency) shift (see section 2.3.3), but many others have been proposed and refined since. Perhaps it is appropriate at this point to state that, current MR temperature imaging methods have not yet been developed enough to overcome all of the drawbacks stated above. Yet it is commonly agreed that MRI,

- Is a noninvasive imaging modality,
- Can achieve high spatial resolution,
- Can be implemented with fast sequences,
- Provides excellent structural imaging on which thermal maps can be overlaid.

Therefore any research on MRTI is performed with the motivation that MR modality is fundamentally more capable than the rest mentioned.

It is the author's opinion that in the next decade, MRTI will be sufficiently developed that it will unquestionably rank the highest among the other existing techniques.

1.2 Outline of the Thesis

Chapter 2 contains background relevant to the methods used in the rest of the thesis. It also includes a brief description of the MRTI techniques from a historical perspective.

Chapter 3 describes the hardware and phantoms used to perform the procedures outlined in this study. It also contains some practical considerations about agar gel preparation.

Chapter 4 is dedicated to phase drift correction. An easy and efficient way to deal with the inherent systematic error of GRE temperature measurement is described in detail.

The key study of this thesis is presented in following chapter. The whole transition from temperature change in the gel to a thermal map on the screen is enclosed in Chapter 5.

Chapter 6 describes an attempt to investigate the effect of different echo times on the efficiency of MRTI. Mean of variance is used as a metric in close correlation with system's thermal resolution.

2. BACKGROUND

2.1 Hyperthermia

Clinical hyperthermia is a broad term which includes any amount of heat application on any portion of the body. Our focus will be Local Hyperthermia (LHT) applied on tumors, which involves the concentration of heat onto a tumor, raising local temperature beyond its physiological thresholds. Falk and Issels conclude in [1] that clinical local hyperthermia treatments on solid tumors is feasible in earlier phases, and they improve response and survival when combined with other treatments such as radiotherapy and chemotherapy at later phases.

There are many different types of cancer that has been investigated for treatment options with hyperthermia. Gonzalez et al. report an increase in complete remission (CR) from 38% to 83% in metastatic melanoma when radiotherapy is complimented with hyperthermia [2].

Due to its tumor location, esophageal cancer can be treated with intracavity heat applicators. Hou et al. report an increase in 2-year survival rate from 20% to 48% with a triple treatment of thermo, chemo and radiotherapy. Ueo and Sugimachi perform a similar study on a larger group of 183 patients [3]. Addition of thermotherapy to the process is observed to increase in 2–year survival rates from 27% to 50% [4].

Van der Zee et al. concentrated their studies on inoperable advanced tumors of rectal, bladder and cervical cancer. Hyperthermia was used in addition to radiotherapy, and the control group received radiotherapy only. Significant increase in complete remission was obtained for cervical and bladder cancer, yet 3-year survival rates did not change for bladder cancer [5].

In localized cancer patients, efficiency of the treatment method is not solely

judged by survival rates and reccurence. In breast cancer, breast conserving interventions may be favored if they achieve close enough results to total mastectomy on these scales. Such interventions followed by chemical or radiation therapy are shown to be capable of even providing a total cure [6]. With the introduction of high field scanners and evolution of imaging techniques, MR breast imaging surpassed the traditional X-ray and US breast imaging methods [7]. With the higher sensitivity, earlier detection of smaller tumors will surely emphasize the importance of less invasive and noninvasive interventions [6].

2.1.1 Types of Hyperthermia

Hyperthermia can be classified according to the modality of heat application. LITT (Laser Induced Thermotherapy), FUS (Focused Ultrasound), RFA (Radio Frequency Ablation) and Microwave ablation are the most commonly used types.

2.1.1.1 LITT (Laser Induced Thermotherapy). LITT is a minimally invasive technique, in which an optical fiber is inserted into the tissue. The tip of the fiber is navigated to the tumor, and energy is applied with a laser beam through the fiber. Since laser and fiber are perfectly compatible with MR imaging, MR guidance is a natural choice for guiding this therapy. Bleier et al. [8], Lai et al. [9], and Harms et al. [10] performed clinical studies with MR guided LITT.

2.1.1.2 FUS (Focused Ultrasound Surgery). FUS or HIFU (High Frequency Focused Ultrasound) uses an ultrasound transmitter to focus sound waves into the tissue. Energy delivered using this technique can be high enough to raise tissue temperature to 90 $^{\circ}C$ at the focal spot in 20 seconds [11]. However creating a thermal lesion with the desired shape and size may take as much as a few hours. Given that the US applicator is MR compatible, MR guidance can be used for targeting, dosimetry [12, 13] and post treatment evaluation [14].

2.1.1.3 RFA (Radio Frequency Ablation). This method uses high frequency electromagnetic waves to induce currents in the tissue. This method has inherent problems such as unpredictability of power dissipation, char forming near electrodes. Also MR guidance of RFA is rather difficult, since EM waves interfere with imaging and create artifacts [6].

2.1.1.4 Microwave Ablation. If the tumor is seated within a fat tissue, microwave ablation can be applied. In breast cancer, microwave energy heats the water content of carcinomas, and it does not have much affect on the surrounding fatty tissue. It is also possible to focus the energy [15].

2.1.1.5 Cryoablation. Cryoablation is a completely different approach from the rest, it uses freezing to ablate the tissue. Application is performed by cooled probes. One interest of this technique to MR imaging is the ease of treatment monitoring. T_2^* shortening of ice makes it possible to image the edges of frozen tissue without post processing. Also, Wansapura et al. developed a method to map the temperature within the frozen ice using eddy current compensated half excitation RF pulses [16].

2.2 Temperature Monitoring Systems

2.2.1 Temperature Imaging with CT

CT numbers obtained via a scan are proportional to local electron density of the subject. It is therefore possible to monitor the temperature of any substance that features a density change under thermal expansion. Fallone et al. found a linear relationship between water temperature and CT number [17]. Sub degree temperature resolutions are possible at CT scan's regular spatial resolution.

2.2.2 Temperature Imaging with US

Ultrasound temperature mapping also utilizes the thermal expansion of tissues. Resulting local changes in the speed of sound can be calculated from tracking the shifts of backscattered sound waves. It has been shown that two dimensional thermal maps can be constructed using this method, with a thermal resolution of less than 1 $^{\circ}C$ [18].

2.2.3 MRTI (Magnetic Resonance Temperature Imaging)

Although CT and US based thermometry methods are still under research, MR is the dominantly used modality. MRI has the following advantages which make it a popular choice:

- It can simultaneously be used for anatomical monitoring [19].
- Temperature dependence of some parameters are tissue independent [18].
- Quantitative measurement is applicable [19].
- It has a potential for high thermal resolution [18].

Also, there are more diverse techniques that have been developed for MRTI. Each method utilizes the temperature dependence of a different MR parameter. A physical discussion about this is given in the following section.

2.3 Physics of MR Parameters

Underlying physical dynamics of MR, therefore all MR parameters are more or less temperature dependent. Such dependence of the following parameters are well documented by various resources:

- Longitudinal Relaxation Time (T_1)
- Diffusion Coefficient (D)
- Proton Resonant Frequency (PRF)

2.3.1 Longitudinal Relaxation Time (T_1)

Temperature dependence of T_1 can be formulated as[20]:

$$T_1 = T_1(\infty)e^{\frac{-E_a(T_1)}{kT}} \tag{2.1}$$

where:

T_1	is the longitudinal relaxation time of the material
$E_a(T_1)$	is the activation energy of the relaxation process
k	is the Boltzmann constant
T	is the absolute temperature

Which can be assumed to be linear in physiological range ($30\ ^\circ C - 100\ ^\circ C$). A direct mapping of measured T_1 values to temperature using the above equation provides absolute temperature measurement. Yet unfortunately T_1 measuring sequences such as inversion recovery or saturation recovery are time consuming (on the order of minutes), thus are not practical for clinical applications.

Different methods are proposed for indirectly mapping T_1. Signal intensity of an RF-spoiled GRE sequence depends on T1 values, and this difference is found to be of sufficient SNR [21]. A faster method with less SNR can be obtained with fast single shot SE trains following an inversion pulse [22, 23, 24].

Though it is technically possible to measure temperature using T1 only, current methods seem to be squeezed between an inefficient trade-off between accuracy and

time [25]. There are several other drawbacks of this approach [20]:

- Temperature dependence of T_1 is dependent on tissue type
- Coagulation produces nonlinear effects
- SNR cannot be increased by increasing field strength (temperature sensitivity decreases)
- Fast sequences measure relative temperature using differences between successive images, and are therefore prone to motion artifacts.

Furthermore, experimental studies suggest that there are strong nonlinear effects based on tissue type, which neither a linear approximation nor Eq. 2.1 predicts [26]. Coagulation is also observed to introduce strong shifts in T_1 values [27, 26]

Figure 2.1 is an empirical plot by [26] showing temperature dependence of T1 values for different tissues.

Still this method may be promising for the imaging of fat tissues, since the superior PRF shift method is not applicable. [28]

2.3.2 Diffusion Coefficient (D)

The thermal Brownian motion of molecules results in an observable motion called diffusion or self diffusion. The rate of this phenomenon is diffusion constant D, and can be measured using MRI. Temperature dependence of this constant is formulated as [19]:

$$D \approx e^{\frac{-E_a(D)}{kT}} \tag{2.2}$$

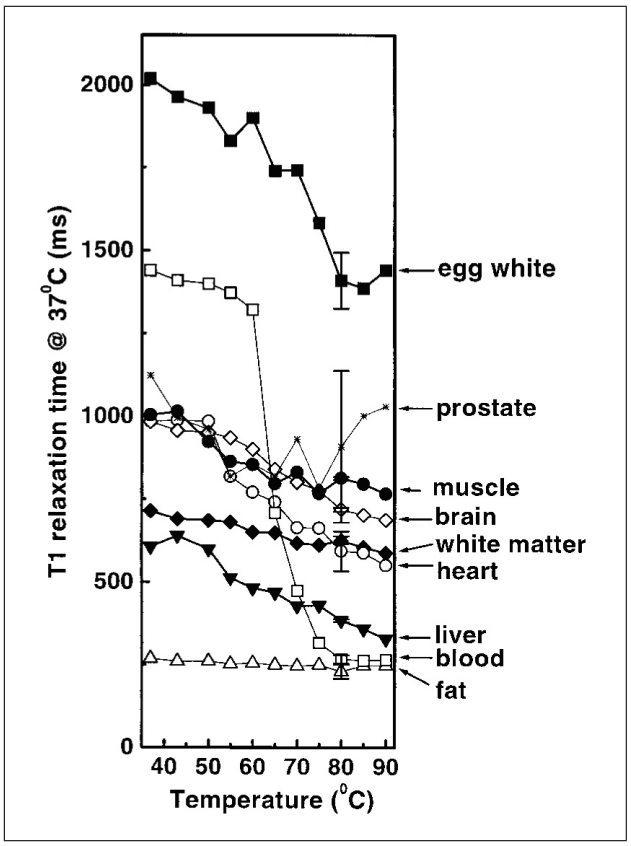

Figure 2.1 Temperature dependence of T1 values for different tissues [26].

where $E_a(D)$ is the activation energy of the molecular diffusion of water, k is the Boltzmann constant, and T is absolute temperature.

This dependence can be used to measure relative temperature differences, but extremely complex nature of water diffusion in the body alone limits the capabilities of this method. An extensive list of drawbacks is included in [20], some of which are listed below:

- Water also diffuses through membrane barriers with diffusion constants much lower than in fluids. Furthermore permeabilities for these membranes are temperature dependent.
- Coagulation greatly lowers diffusion constant, which may be interpreted as a large temperature difference.
- Method is prone to motion artifacts.

- Lipid suppression is required since low D of lipids is a potential source of artifacts.

Especially the first two inconveniences significantly reduce the efficiency of diffusion constant based methods for in vivo applications.

Figure 2.2 is an empirical plot by [26], showing temperature dependence of ADC (apparent diffusion coefficient) values for different tissues.

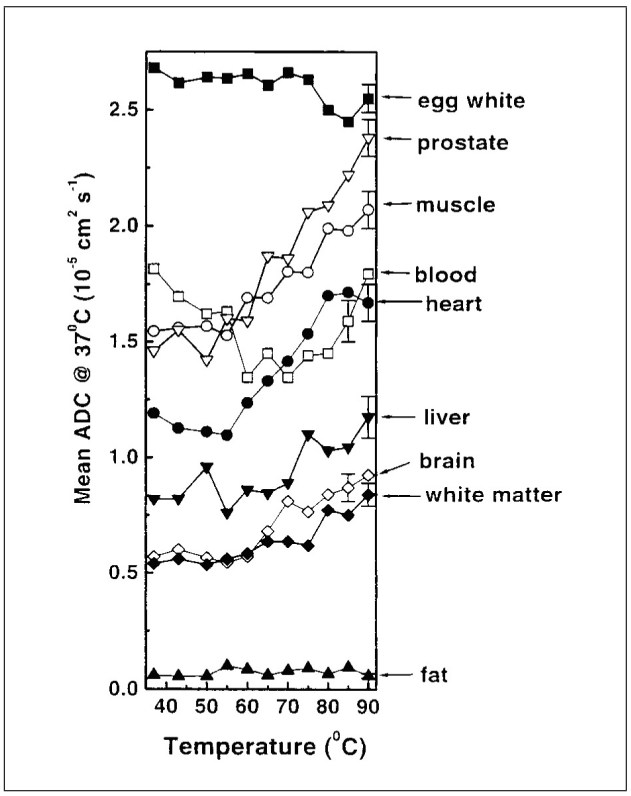

Figure 2.2 Temperature dependence of ADC (apparent diffusion coefficient) values for different tissues [26].

2.3.3 Proton Resonance Frequency (PRF)

Proton Resonance Frequency (PRF) shift, or in other words chemical shift of water is though to originate from local shielding effects of the molecules themselves. Molecular dynamics of this phenomenon is quite complex, and is not discussed here. Interested reader can refer to [29, 30, 31, 32] for a core physical description of possible

molecular interpretations. These research sought a better understanding of water's molecular dynamics, and tried to fit temperature dependence data of PRF shift to probable models. In 1966, Hindman concluded that PRF shift cannot be explained by a single model [32].

Nevertheless, to utilize PRF shift for temperature measurement purposes, it is possible to overlook the theoretical basis, and approach the subject from an empirical standpoint.

In general, a calibrating curve can be obtained for a substance type, or better yet one can be found from numerous studies in literature, as provided by [32] and reprinted here as figure 2.3.

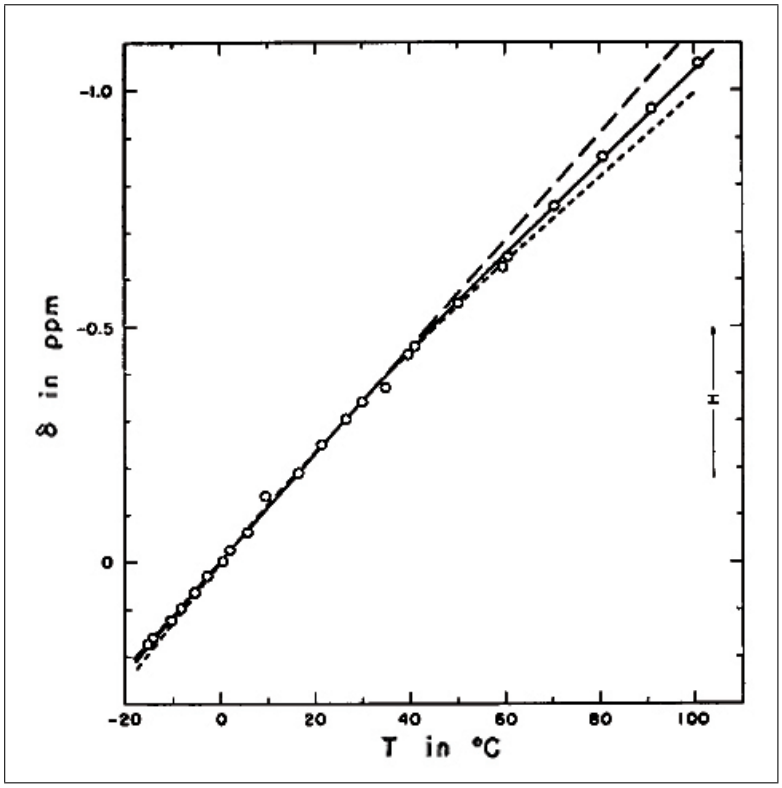

Figure 2.3 Chemical shift of water vs. temperature. (o-o) experimental data, (–) straight line, (- -) susceptibility corrected line [32].

Temperature dependence of water PRF shift is calculated to be around $0.01 ppm/°C$, and this value forms the basis of MR thermometry. Yet although this shift can be easily measured with spectroscopic techniques, spatial mapping of spectroscopic data requires

indirect approaches.

We have discussed that molecular mechanisms create magnetic shielding, deviating the local magnetic field strength, and consequently shifting the resonating frequency of the protons. Therefore any measured shift will be a result of not only molecular effects, but also of magnetic field inhomogeneity. Mathematically speaking:

$$\Delta B_0 = \partial B_0(\vec{R}) + B_c(T(\vec{R})) \tag{2.3}$$

in which:

$\vec{R}$	is the spatial vector
$T(\vec{R})$	gives the temperature distribution
$\partial B_0(\vec{R})$	is the change due to inhomogeneity
$B_c(T(\vec{R}))$	is the change due to the chemical shift
ΔB_0	is the total change in the magnetic field

In 1992, Ishihara et. al. [33, 34] proposed an MRI technique to noninvasively measure spatial temperature distribution. Field inhomogeneity can be mapped to phase difference images using various MR sequences.

Ishihara's method is as follows:

1. Obtain a reference phase image at

   $T = T_0$

   The total local field inhomogeneity will correspond to:

   $\Delta B_0(T_0(\vec{R})) = \partial B_0(\vec{R}) + B_c(T_0(\vec{R}))$

2. Obtain another phase image at an arbitrary temperature, T .

   The total local field inhomogeneity will correspond to:

   $\Delta B_0(T(\vec{R})) = \partial B_0(\vec{R}) + B_c(T(\vec{R}))$

3. Take the difference of these images to cancel the effect of change in field due to inhomogeneity $\partial B_0(\vec{R})$

   Difference image will correspond to:

   $\Delta B_c(\Delta T(\vec{R})) = B_c(T(\vec{R})) - B_c(T_0(\vec{R}))$

4. Variations in local magnetic field causes a difference in resonance frequency of the protons. When the same protons are imaged at different temperatures, their varying speed causes the images to have slightly different phase values. The relationship between this phase difference and temperature depends on the sequence type and sequence parameters. For gradient echo imaging, it is governed by the following equation:

$$\Delta T(\vec{R}) = \frac{\Delta\theta(\Delta T(\vec{R}))}{\alpha\gamma \cdot TE \cdot B_0} \tag{2.4}$$

   in which:

α	is the temperature dependence coefficient of the material
γ	is the gyromagnetic ratio
TE	is the echo time
B_0	is the field strength

   Equation 2.4 is all we need to convert $\Delta\theta$ values to ΔT values

The procedure above, originally presented in 1992, is still used today as a research tool. The advantages of this method are:

- Near independence of tissue type

- Linear dependence on temperature
- Fast acquisition

Main disadvantages would be:

- It is affected by temperature dependent changes in magnetic susceptibility
- PRF shift is not observed in lipids
- It is prone to motion artifacts

2.4 GRE (Gradient Recalled Echo Imaging)

Gradient recalled echo is an imaging technique which utilizes smaller rotation angles and refocusing gradient pulses to decrease acquisition time. Figure 2.4 borrowed from [35] contains the sequence diagram of a basic GRE sequence. A slice selection gradient (G_s) of an arbitrary angle is applied first. Then phase encoding and dephasing frequency encoding gradients (G_ϕ and G_f) are applied at the same time. This has the effect of selecting a line within the slice, and applying frequency coding to the points along the line. Following immediately, a rephasing frequency encoding gradient refocuses the signal, and an echo is obtained. Due to its timing advantage, it is mostly used in fast sequences and 3D acquisitions. Also, its sensitivity to magnetic field inhomogeneities makes it easier to map small resonance frequency deviations to temperature.

2.5 Phase Drift

De Poorter et al. reports a phase drift phenomenon observed during lengthy and repetitive acquisitions of thermal mapping, and they propose two different methods for compensating it in [36] and [37].

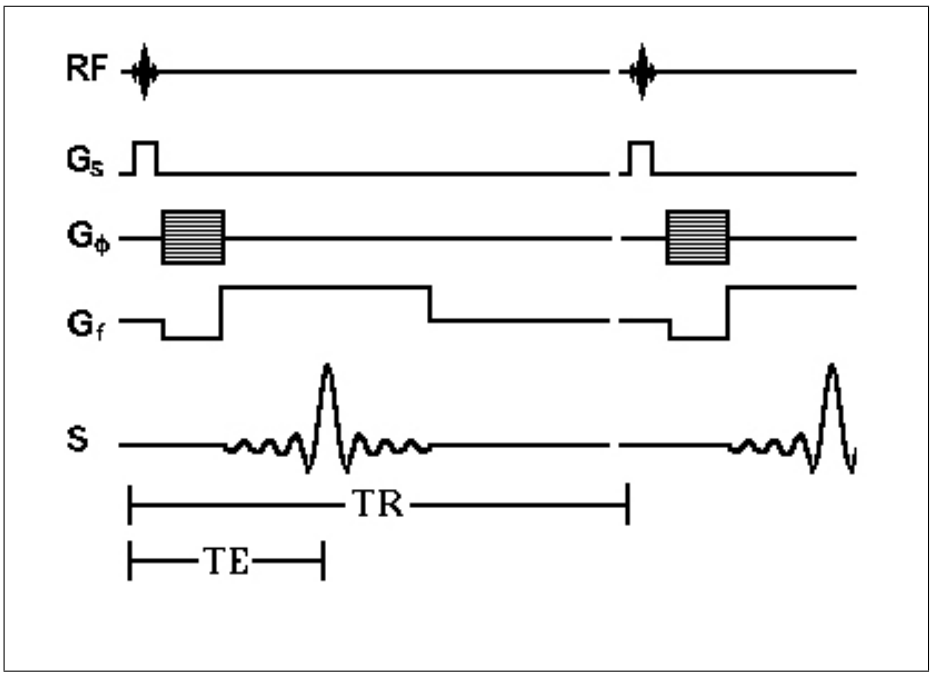

Figure 2.4 Timing diagram of a gradient recalled echo (GRE) sequence [35].

The drift is caused by the temporal instability of the external magnetic field, and is of hardware origin. The instability causes only slight deviations in resonance frequencies of protons, thus produces no noticeable inconveniences for magnitude images. However, those slight deviations are interpreted as temperature difference with temperature mapping sequences [37].

Both of proposed methods use constant temperature reference phantoms to asses the distribution of the drift, so that it can be subtracted from the rest of the image. First method [36] assumes that the drift is constant, while the second one assumes it is has first order linear nature over the entire region [37]. Poorter et al. also showed that the second one was more accurate, his demonstration is reprinted here as figure 2.5.

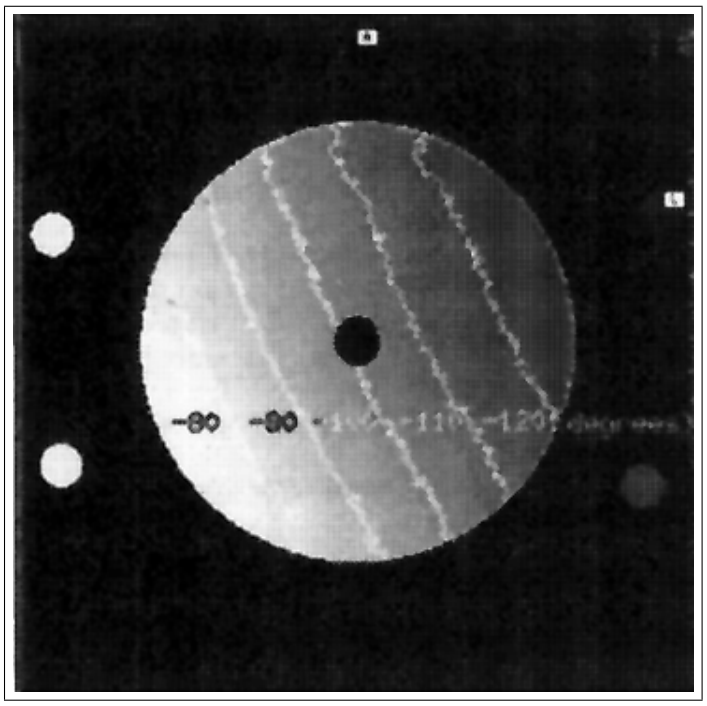

Figure 2.5 A phase difference image with iso–phase contours of $-80°$, $-90°$, $-100°$, $-110°$, $-120°$. The contour configuration supports the assumption that the spatial phase drift is linear over the image [37].

2.6 Further Studies on PRF Methods

PRF based MR thermometry has proved to be superior against the others on most scenarios [20, 19]. Thus most of the contemporary research has focused on ways to overcome its problems. Main three problems regarding this method are motion artifacts, inexistence of chemical shift in lipids, and proneness to temperature dependent changes in magnetic susceptibility, as listed in section 2.3.3. So far the method fails to provide a solution to measuring temperature change in lipids, but any lipid based artifacts can be eliminated by lipid suppression if the tissue of interest does not contain lipid components.

There are many ways to handle motion artifacts in general MRI, and Senneville et al. published a series of suggestions between 2003 and 2005, focusing specifically on thermal mapping. They demonstrated that real-time algorithms are feasible for real–time correction of motion and geometric distortion artifacts. Their method involves post processing of acquired magnitude images to extract transformation matrices [38].

Further work revealed that the motion correction scheme can be applied to 3D acquisitions, giving successful real time correction of respiratory motion [39]. Finally, they successfully implemented and demonstrated an atlas based motion correction method for thermal mapping of human kidneys [19]. Different parties also provide similar methods to overcome motion artifacts in real time [40, 41].

Referenceless PRF shift thermometry also emerged as a method to overcome motion artifacts. Phase differences can be estimated from a single image, based on the phase of a distant region of constant temperature. Phase from this reference region is extrapolated to the entire image to serve as background phase. This method eliminates motion problems completely, though introduces some others [42, 43, 44].

Susceptibility artifacts are more pronounced when external applicators are used, as in RF ablation. Boss et al. demonstrates worst case scenarios in [45], and Shmatukha et al. suggests ways to correct them [46].

2.7 High Frequency Focused Ultrasound (HIFU)

MRTI can be used with any MR compatible heating method, but High Frequency Focused Ultrasound (HIFU) deserves a separate section (also known as Focused Ultrasound (FUS)). Ultrasound heating combined with MR monitoring provides many advantages for non–invasive tumor treatment. MR provides excellent anatomical imaging prior to the intervention, which enables target localization. Ultrasound transducers are capable of focusing high frequency sound energy at a single point, even deep seated tumors without serious collateral damage. Use of transducer arrays is also possible. Thermal monitoring with MRTI during intervention ensures proper targeting, dosimetry, damage control and verification of treatment. Research on MR guided HIFU has increased in the last few years, since there are now FDA approved MR compatible HIFU systems available for certain procedures.

Contemporary research has diversified to assess the requirements of different

types of cancer. Uterine fibroids has FDA clearance to be treated with MR guided FUS. Tempany et al. performed the first clinical trial on 6 uterine leiomyomas patients, concluding that the method was both feasible and safe [47]. Hesley et al. provide a research with 42 patients with uterine fibroids and report decrease in bleeding and pressure symptoms [48]. Pilatou et al. study the usage of diffusion weighted imaging for pre-planning and verification [49]. All of these parties use PRF shift as their MRTI method.

Traditional brain surgery has many complications, thus brain is another popular anatomic region for non-invasive treatment. Though researches with human subjects are yet to be performed, McDannold et al. show possibility of MR guided FUS on primates. Post operational imaging and pathological findings suggest that FUS therapy can be safely used for regions as much as 4.8 cm deep without damaging the surrounding tissue. They do report however, some regional limitations caused by skull heating due to the high absorption characteristics of the skull [50]. Stafford et al. report similar findings on a canine model [51].

Body cavity transducers have been developed to enable ultrasound energy development into specific regions of the body. Chopra et al. use a trans urethral ultrasound transducer on a canine model for prostate gland ablation [52].

It should be noted that HIFU with MRTI is not restricted to ablation interventions. There are also experimental studies in using ultrasound to disrupt blood–brain barrier for localized drug delivery [53, 54], and control of transgene expression [55].

3. EXPERIMENTAL SETUP

3.1 Overview

The setup used consists of two parts; a hot water circulating system, and a modular gel phantom to which water circulation can be connected. Both parts are made from scratch, using equipment available at hardware and medical stores.

3.2 Water Heating and Circulation

The overall goal was to come up with an affordable system which can heat a gel phantom placed in the magnet of the scanner. Following are the design criteria and restrictions:

- All control switches and machinery should remain in the control room.
- All parts residing in the waveguide and exam room should be MR compatible, and watertight.
- System should withstand prolonged periods of working with high temperature
- Heater should be able to create a final temperature difference of at least $30°C$
- Heating rate should be high enough to create a noticeable temperature gradient within the gel

Figure 3.1 contains a simplified diagram of the heater/circulator.

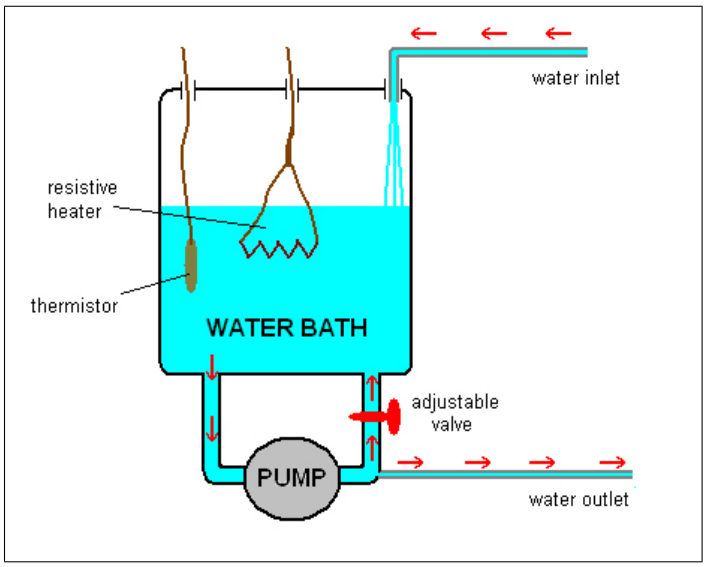

Figure 3.1 Simplified block diagram of hot water circulator

3.2.1 Materials

After many trials and failures, the following materials were found to be suitable:

- House grade boiler circulation pump
- Flexible PVC garden hose
- Aluminum shower hose casing
- Dipping style water heater (450 Watts)
- Thermostat (range: 30 $°C$ - 110 $°C$)
- Aquarium grade air hose and connectors($\phi = 4mm$)
- On/off switches
- Brass piping connectors (between the pump and hoses)
- Cables and electrical connections
- Hardboard and screws for the casing

3.2.2 Description

The setup needs to be easily portable to and from the exam room, so it is enclosed in a hardboard casing as shown in figure 3.2. The box was constructed so that it could remain closed for the duration of the exam, which usually took about an hour. Power and piping connections are left outside of the box for this purpose. There are three control switches on the top of the box. A thermostat control to adjust temperature, a switch to supply main power to the system, and another switch that turns the pump on and off. As a black box, this system is capable of circulating hot water at an adjustable constant temperature up to 100 $^{\circ}C$.

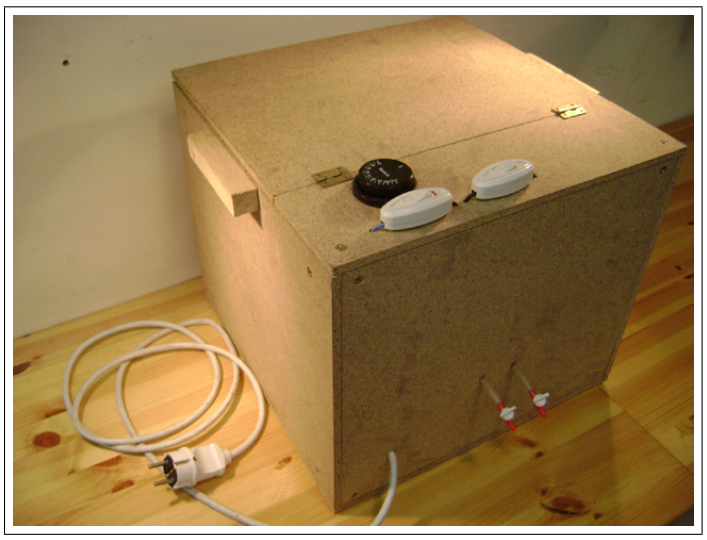

Figure 3.2 Outside appearance of the hot water circulator

Inside of the box is a little more complicated, as seen in figures 3.3 and 3.4. There are two main water hoses in the water bath, connected to the pump. When the hot water feed to the phantom is closed using the little red valves seen on the side of the box in figure 3.2, the pump still works circulating the water within the box itself. Main reason for this is to reduce the load on the pump, which is not designed to handle circulation on such a thin piping system. This bypass system also has some other benefits. As seen in figure 3.4, heating is performed from a single point using a resistance, and large scale circulation within the bath ensures uniform temperature distribution throughout the system. Furthermore, the bypass connection has a valve on it, that when closed slightly, raises the pressure within the pump and increases the

Figure 3.3 Inside of the hot water circulator

hot water flow rate to the phantom.

3.3 Phantom

All phantom gel used for this thesis is composed of 3% Agar and $2mM\ CuSO_4$ in a water base. Three sets of scans were performed to calculate its relaxation constants. Calculated values and corresponding sequences are given in table 3.3. All calculations were performed with the curve fitting toolbox of MATLAB.

3.3.1 Gel Preperation

Agar is a powder in its dry form. It is mainly used as a gel base in many research techniques and also in food industry. Many different types are available to cope with different demands of microbiology research, however most of these are high purity agar mixed with a specific nutrient. In our case, we only needed the gel forming structure of it, so we used food grade pure agar. The procedure outlined below is fairly simple, and can be carried out with household equipment if there is no access to a wet lab.

Figure 3.4 Inside of the water tank

Equipment and Materials:

- Heater plate with magnetic stirrer
- Glass rod for manual stirring
- Balance
- Glass beaker with volume markings
- Injector ($5mL$ or less)
- Thermometer
- Agar
- Copper Sulphate ($CuSO_4$)
- Distilled/Deionized water

Preperation:

Constant	Seq.	Sequence Parameters (ms)	Calculated Value
T_1	SE	$TE = 15$ $TR = 125, 250, 500, 1000, 2000, 4000$	346 ms
T_2	SE	$TE = 12, 15, 19, 23, 29, 37, 46, 57, 72, 89, 112$ $TR = 1000$	42 ms
T_2^*	GRE	$TE = 4, 8, 16, 32, 60$ $TR = 200$ $\alpha = 30°$	35 ms

Table 3.1
Calculated relaxation values of Agar gel with 3% Agar and $2mM$ $CuSO_4$

1. Measure the required amount of Agar. Keep in mind that Agar percentages are by mass, i.e. 3% Agar solution is obtained by disolving 30 $grams$ of Agar in 970 $grams$ of water.

2. Necessary amount of $CuSO_4$ will be too small to be measured without a very sensitive scale and lab conditions. Unless you are preparing a large quantity of gel measured in liters, the following method ensures easier and more precise results:

   (a) Calculate at what concentration will the addition of $1mL$ $CuSO_4$ solution to the total of your prepared gel will raise the $CuSO_4$ concentration of your gel to the required value. Say this value is X.

   (b) Measure the smallest amount of $CuSO_4$ you can safely measure, and prepare an X Molar $CuSO_4$ solution with adequate water.

   (c) Fill your injector with this solution.

   (d) You will be adding $1mL$ of this to your gel before it is left to cool down.

3. Mix Agar powder and enough water in the beaker. Make sure you have a mark at exactly the amount of total gel you will prepare.

4. Start heating and stirring on the magnetic stirrer plate. Use the glass rod to stir once the gel becomes too thick to be sufficiently stirred from below. Adjust

heat or stir faster if necessary to prevent burning the mixture at the bottom. An alternate is to heat the mixture in boiling water.

5. When the powder has fully dissolved (the gel is no more cloudy) and the temperature exceeds at least 90 $°C$, add 1 mL of your $CuSO_4$ solution, and replace the missing amount (due to evaporation) with hot water.

6. Pour the gel into the final container of your choice. You may wish to wait for it to cool down slightly, but keep in mind that the gel starts to solidify around 70 $°C$

3.3.2 Phantom casings

Two different geometries were used for gel containers, 50 mL cylindrical tubes and 500 mL rectangular blocks.

The rectangular block phantom seen in figure 3.5 has a uniform interior and is heat insulated with 1cm styrofoam. It is used for relaxation constant measurement (table 3.3 in section 3.3) and the validation of drift correction scheme (chapter 4).

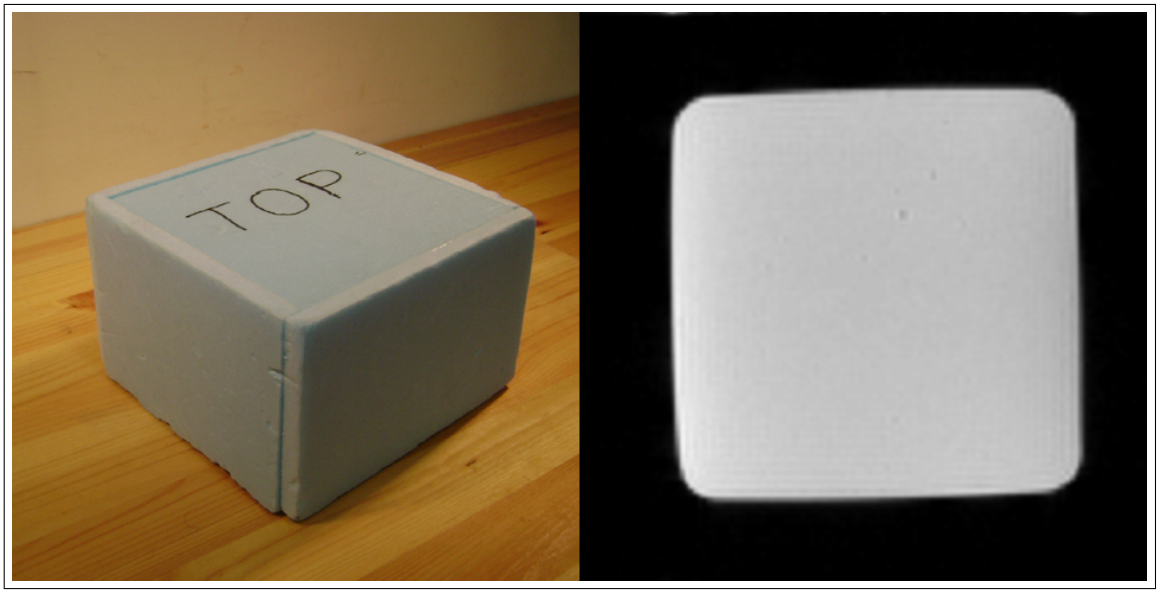

Figure 3.5 Rectangular Phantom. Picture and MR image

Cylindrical tubes are used for temperature measurement experiments. Drift correction scheme described in chapter 4 requires reference signals of constant temperature, and the temperature measurement requires the heating of a tube with circulating hot water. Figure 3.6 shows a reference tube, and figure 3.7 shows one that is to be heated.

Figure 3.6 Tube of Agar gel to be used as reference

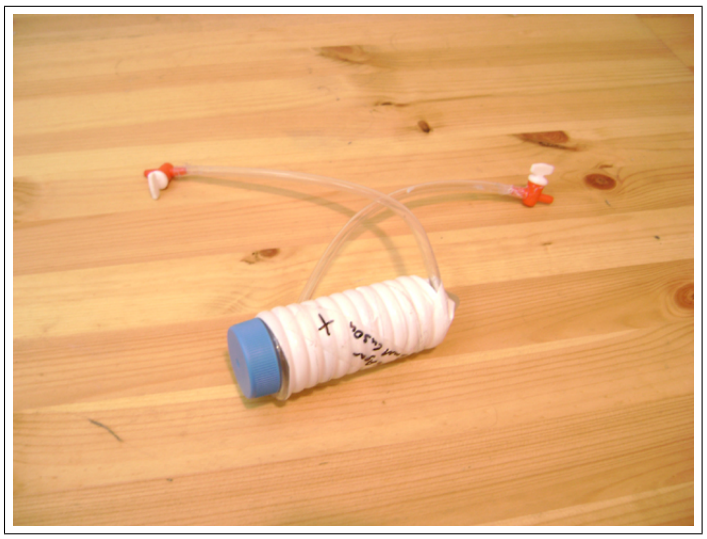

Figure 3.7 Tube of Agar gel to be heated during scan

A pattern of one in the middle and four in the corners were used. Reference phantoms are placed in the corners so that they span the entire imaging field of view. A foam case was constructed to hold the tubes in place and also to insulate all tubes individually. This case, seen in figure 3.8 is designed so that the tubes can be inserted

and removed with ease, as depicted in figure 3.9. This way, a second experiment can immediately be performed by replacing just the tubes. Finally, figure 3.10 shows final appearance and MR image of this phantom.

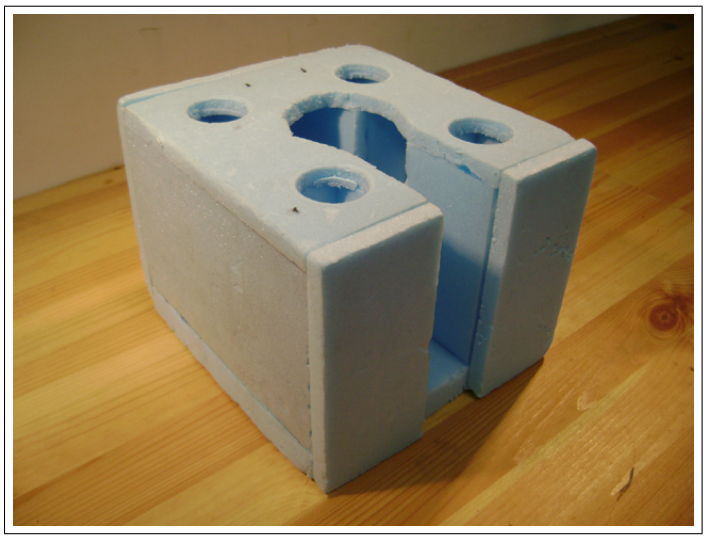

Figure 3.8 Foam case for tube phantoms

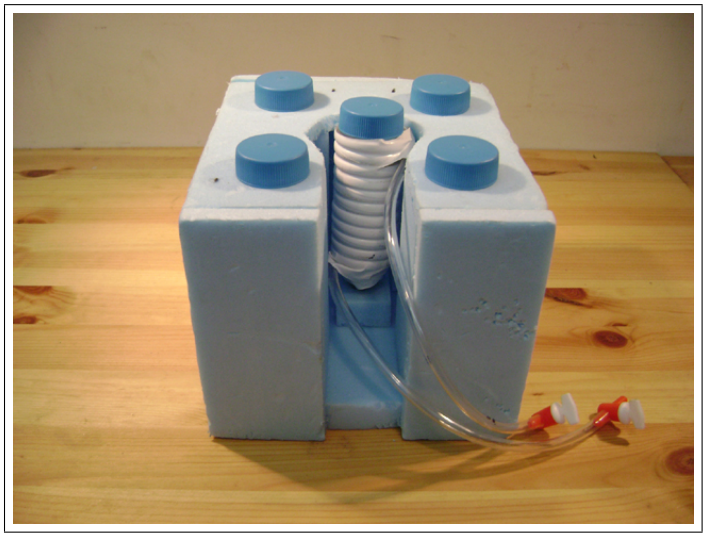

Figure 3.9 Case with tube phantoms in place

The two sections of the experiment setup are described in sections 3.2 and 3.3 respectively. The heater is placed in the control room, and the phantom is placed in the magnet. Water circulation between them is carried out through aquarium grade air hose ($\phi = 4mm$) which enters the exam room through the waveguide. Validation of this system is presented in the following section.

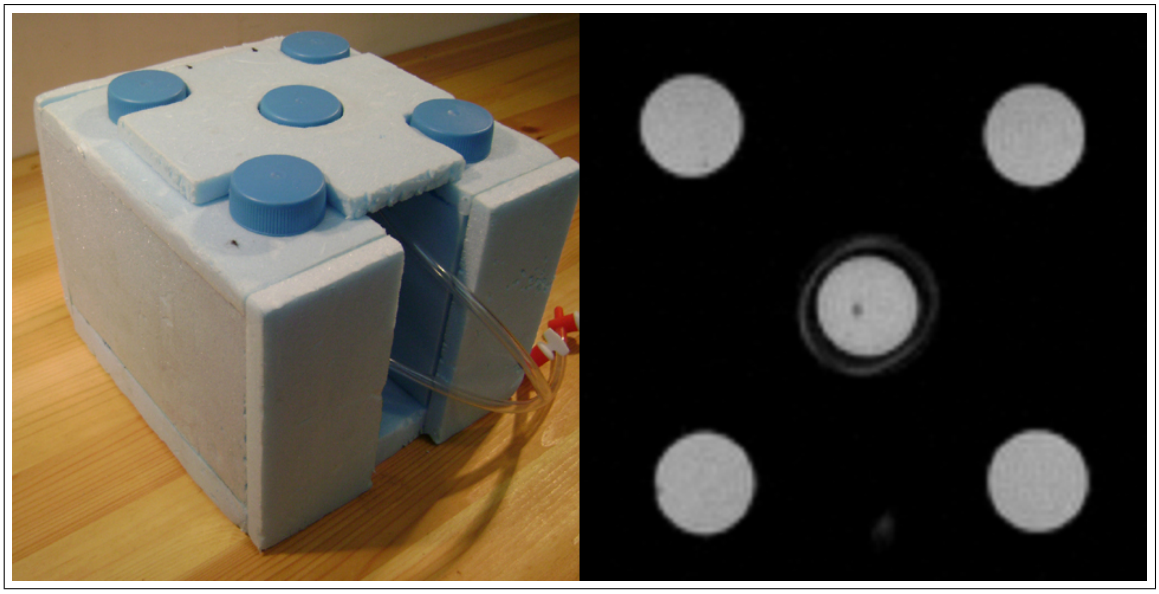

Figure 3.10 Final look of the case and the tube phantoms. Picture and MR image

3.4 Validation Experiments

Validation experiments were performed before the setup was taken to a scanner room. Overall goal of these trials were to make sure the system could do what it was designed for, without putting the personnel and equipment in danger. Temperature measurements were also performed to evaluate the heating capacity and dynamics of the system. Two consecutive experiments were performed, the first one (section 3.4.1) indicated some problems with the hardware. These were patched and the second experiment (section 3.4.1) ensured that the setup was fit to be taken into the scanner room.

3.4.1 General Validation

Some setups prior to the final configuration were highly problematic, non-durable, and prone to spontaneous malfunctions. Testing of the individual components resulted in some design changes, patches, and material type replacements. A final trial is conducted to ensure proper operation of the system as a whole. Specific points of interest for this trial were:

- Establishment of a solid protocol to be used during MRTI
- Testing the system in terms of the following:
  - Ability to withstand continuous functioning for at least 1 hour.
  - Ability to sufficiently increase the gel temperature (at least 30 $^{\circ}C$)
- Measurement (or quantitative analysis) of the following:
  - Temperature difference between outlet and inlet temperature. If this value is measured to be more than acceptable, measures will be taken to either speed up the circulation, or to insulate the piping.
  - Maximum temperature in gel's center

– Time required for a specific change in gel temperature.

The experiment is performed almost as it would have been in an MRI environment with the exception of attached thermometers. Figure 3.11 shows a simple diagram and temperature measurement locations for this experiment. The step by step procedure is presented in the Results section.

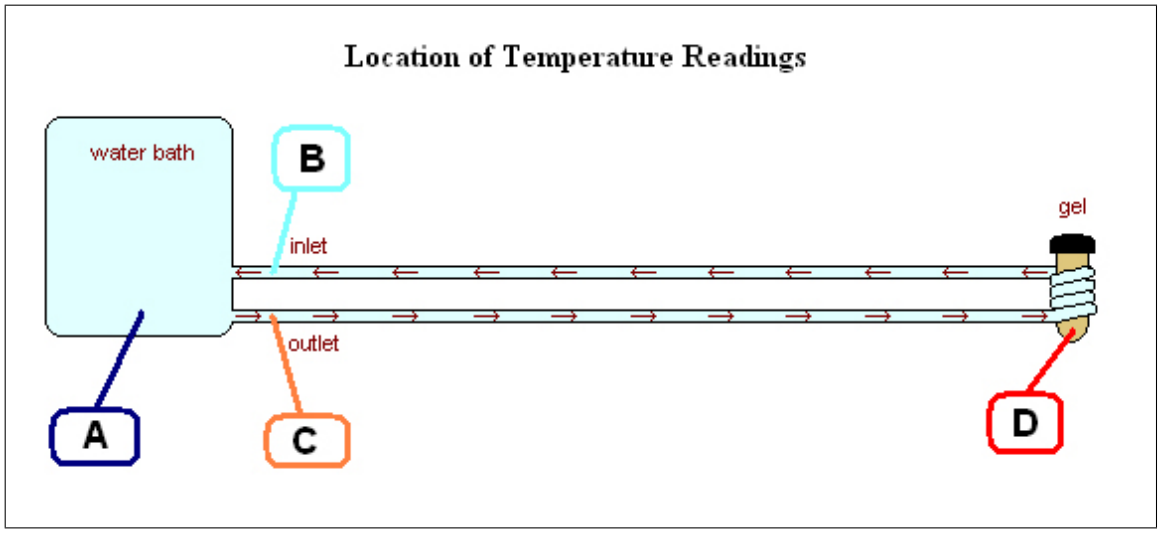

Figure 3.11 Setup diagram and location of temperature readings

3.4.1.1 Results. Since this thesis will involve multiple imaging sessions, it is very important to establish a protocol to ensure comparability of data acquired in different sessions. The one listed below was found to be convenient for our case. Some of the items are specific to the experiment setup, and will not be needed with another design.

Protocol:

1. Make sure both switches are off and the thermostat is set to 0 $^{\circ}C$.
2. Place the black-box (heating system) on the same level as the gantry, and connect to a 220V power supply.
3. Place the gel in the gantry and connect the piping accordingly.

4. Fill the bath with cold water. It will take approximately 5 liters.
5. Close all (3) valves of the pump.
6. Fill inlet and outlet hoses of the pump with water, and place rubber stoppers on the ends.
7. Immerse the hoses in the water bath and remove the rubber stoppers. Take care to keep air out of the hoses.
8. Start the pump by pressing both switches.
9. Open the valves corresponding to the hoses and verify circulation in the water bath.
10. If everything is all right, properly and securely position the pump inside the black-box.
11. Open the hot water outlet valve to fill the piping with water. Circulation speed can be increased by partly closing the valve corresponding to the large hose going back to the water bath. Closing this valve exactly 'half way' results in good circulation in both loops.
12. When all the air has drained out of the system, and you feel like ready to begin, start heating the water by turning the thermostat up to 90 $^{\circ}C$.
13. Take measurements for the following 60 minutes.
14. Turn off and carefully dismantle the system.

Data:

The chart shown in figure 3.11 was obtained with the temperatures measured at locations A through D.

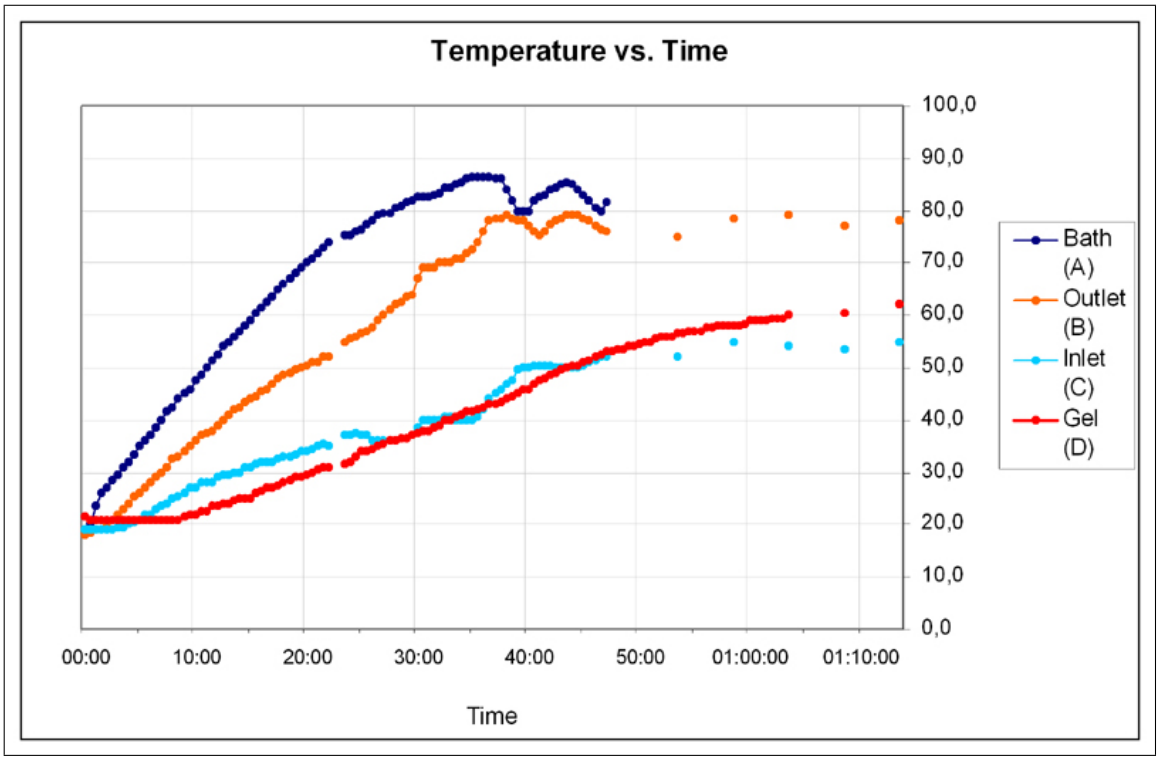

Figure 3.12 Temperature vs. Time readings at various points of the setup

3.4.1.2 Conclusion. A detailed protocol was established, which was refined by the next validation and then used for all of the consequent experiments.

One of the design criteria was continuous functioning for 1 hour. In this trial, the system functioned for a period of 75 minutes, in one piece, with the following exception: After the water reached some temperature (plots suggest around 65 $°C$ and roughly 18 minutes) large hoses became extremely elastic, and collapsed at curvatures. This, unnoticed until the end, blocked one of the circulation loops (internal loop, not shown on the diagram). The purpose of this internal loop was to reduce the strain on the pump, to stir the water bath, and to ensure fast circulation through the pump to minimize temperature drop in the pump. Respectively, the pump worked under heavy load for about 60 minutes but with no observable loss of function. Water in the bath was not uniform in terms of temperature causing the outlet water temperature to be less than the value at the thermostat read point. Water passed through the pump very slowly, its temperature dropping. Hence outlet temperature was well below bath temperature until after $t = 35$ minutes. To prevent this inconvenience in consequent

trials, flexible aluminum hose casings were installed within the hoses to prevent them from collapsing even when they loose their rigidity.

Temperature in the middle of the gel was increased from 20 $^{\circ}C$ to 60 $^{\circ}C$, which is more than sufficient for this study.

No change in gel temperature was recorded until 10 minutes into the procedure. Then the temperature increased almost linearly at a rate of 0.8 $^{\circ}C/min$, until it began to stabilize toward 60 $^{\circ}C$.

The temperature was taken from a single point in the gel, therefore we have no data on the temperature distribution within the phantom. If the material is heated slow enough and its temperature diffusion coefficient is relatively high, then temperature inside the phantom will practically be uniform at all times. Since our ultimate goal is to image the temperature distribution, we need to avoid uniform heating at some point. There is some evidence in the results that the phantom was not uniform in terms of temperature for this trial, and this was investigated further in the next validation study.

As an unexpected but favorable result of this study, the system turned out to be quite robust in terms of transferring heat to the phantom. Numerous effects disrupted ideal operation of the system during the procedure, and there is an inevitable ripple in the water bath temperature due to the nature of the thermostat feedback system used, however the graph shows that increase in gel temperature is almost as consistent as one can hope for.

As a result, the system was found to be satisfactory, though there was improvements made to make circulation hoses non collapsible, and also another validation experiment was deemed necessary before the setup will be utilized in an MRI environment.

3.4.2 Step Response

Functioning of the 'gel heating setup' was verified previously (see 3.4.1). This second simulation is performed to obtain the step response of the heating system, and to verify the methods to overcome some difficulties encountered in the previously. In the previous simulation, after the water reached some temperature (plots suggest around 65 $°C$) large hoses became extremely elastic, and collapsed at curvatures. This resulted in several complications, such as extreme temperature drop over the pump, and unstable water bath temperature. These parts were replaced and enhanced. Their durability will be verified in this experiment. Specific goals of this simulation are as follows:

- Testing the system in terms of the following:
  - Ability to withstand high water temperature. (> 80 $°C$)
- Measurement (or quantitative analysis) of the following:
  - Step response of the system.
  - Highest possible rate of change in temperature. (dT/dt)
  - Passive cooling of the gel.

A slightly different protocol is used to heat the water beforehand and keep the circulating water temperature constant during heating. This protocol is presented in the next section. Also, the number of temperature recordings is decreased to two. Their places are shown in figure 3.13.

3.4.2.1 Results. Protocol:

1. Make sure both switches are off and the thermostat is set to 0 $°C$.

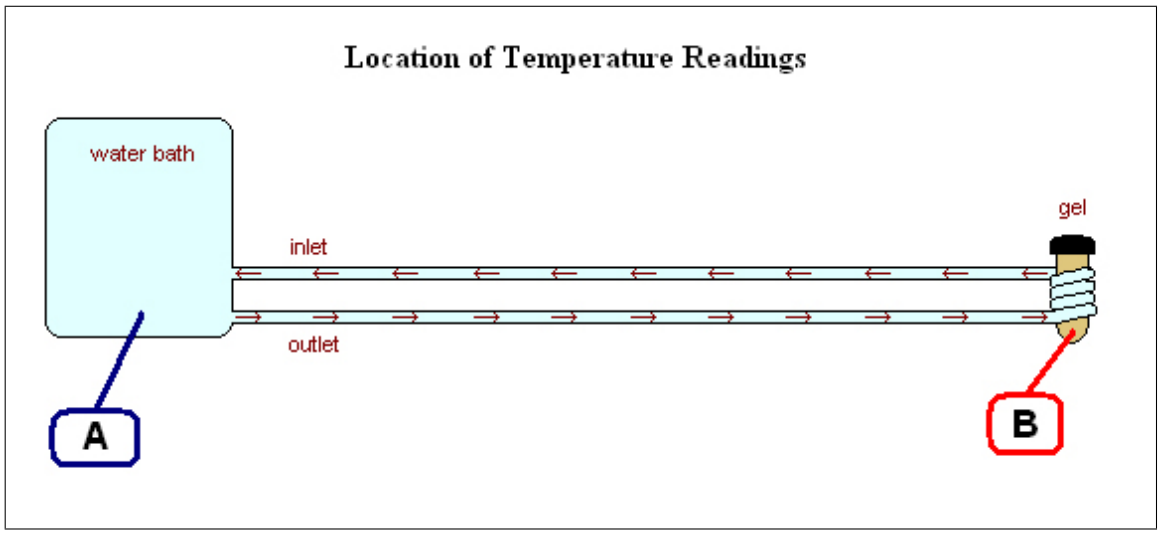

Figure 3.13 Setup diagram and location of temperature readings

2. Place the black-box (heating system) on the same level as the gantry, and connect to a 220V power supply.

3. Place the gel in the gantry and connect the piping accordingly.

4. Fill the bath with cold water. It will take approximately 5 liters.

5. Close all (3) valves of the pump.

6. Fill inlet and outlet hoses of the pump with water, and place rubber stoppers on the ends. Immerse the hoses in the water bath and remove the rubber stoppers. Take care to keep air out of the hoses.

7. Start the pump by pressing both switches.

8. Open the valves corresponding to the hoses and verify circulation in the water bath.

9. When all the air has drained out of the system, and you feel like ready to begin, start heating the water by turning the thermostat up to 90 $^{\circ}C$.

10. Wait until the water in the bath has reached the desired temperature.

11. Open the hot water outlet valve to fill the piping with water. Circulation speed can be increased by partly closing the valve corresponding to the large hose

going back to the water bath. Closing this valve exactly 'half way' results in good circulation in both loops.

12. Take measurements until the gel temperature exceeds 60 $°C$, and then turn off the hot water circulation.

13. Turn off the system completely.

14. Continue to take measurements until the gel temperature drops sufficiently.

15. Dismantle the system.

Temperature at two different points were monitored for a duration of 90 minutes. Figure 3.14 contains the results as a chart.

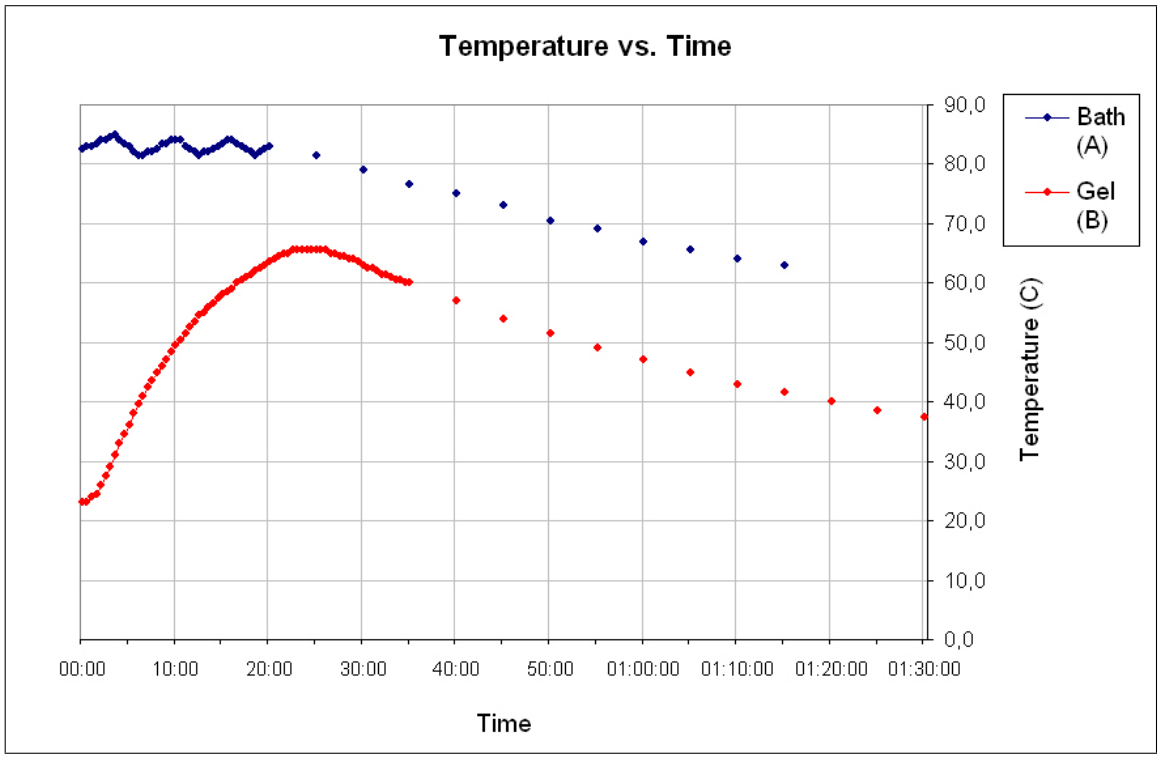

Figure 3.14 Temperature vs. Time readings at various points of the setup

3.4.2.2 Conclusion. The protocol from the previous validation was refined, and used for the rest of the experiments as it is presented here.

One mechanical failure of the previous trial was the collapsing of the plastic hoses when exposed to temperatures above 65 $°C$. With the addition of aluminum support, this ceased to be a problem.

The measurements in the first 20 minutes can be considered the step response of the system, since the phantom is subject to a constant hot water temperature. Figure 3.14 shows this response graphically. Also, rate of change in temperature (dT/dt) was also calculated from the measured data as shown in tables 3.2 and 3.3:

Temperature Range ($°C$)	Avg. rate of change (dT/dt) ($°C/min$)
$30 < T < 40$	3.3
$40 < T < 50$	2.4
$50 < T < 60$	1.5

Table 3.2
Maximum rate of change obtained during heating with the setup

Temperature Range ($°C$)	Avg. rate of change (dT/dt) ($°C/min$)
$60 < T < 50$	0.55
$50 < T < 40$	0.36

Table 3.3
Rate of change for passively cooling tube phantom

Cooling is observed to be significantly slower than heating. A related issue worth noting is that water bath temperature was always above the gel temperature and with a slower cooling rate. This means that if water circulation is to be used to cool the gel actively, water in the bath needs to be cooled first, either by replacement or any other method.

As a result, significant heating rate can be achieved by delaying the circulation until temperature in the water bath reaches a high point.

Although a single thermometer is used to collect data from within the gel, the results show that a measurable radial temperature gradient is present throughout the gel, since the temperature at the center of the gel does not reach its peak value until 5 minutes after the circulation is stopped, with an additional 2 $^{\circ}C$ to gain.

Together with the results previous simulation, it is safe to say that this system is suitable for MRTI experiments.

4. PHASE DRIFT CORRECTION

In an attempt to observe and correct the phase drift phenomenon described in section 2.5 on page 16, a phantom study was performed. A $10cm \times 10cm \times 2cm$ rectangular block of homogeneous agar phantom (3% Agar, $2mM$ Cu_2SO_4) was prepared and enclosed in a heat insulating case (Figure 4.1).

Figure 4.1 Rectangular gel phantom with heat insulation

Phantom was left in the exam room for 2 hours to let it reach thermal equilibrium. Three sets of acquisitions were performed, respectively in coronal, sagittal, and transverse planes using the head coil. The phantom was rotated before each set such that the same physical cross section was excited.

Each acquisition set consists of GRE scans ($\alpha = 30°$, $TE = 15ms$, $TR = 29ms$) with one minute intervals for a duration of 30 minutes.

4.1 Data and Analysis

Phase difference images were generated by subtracting the first phase frame from the entire set. One dimensional unwrapping was performed to remove phase

discontinuities. Phase evolutions of the sets are visualized in figure 4.2. Each layer is median filtered prior to drawing to enhance visual perceptibility.

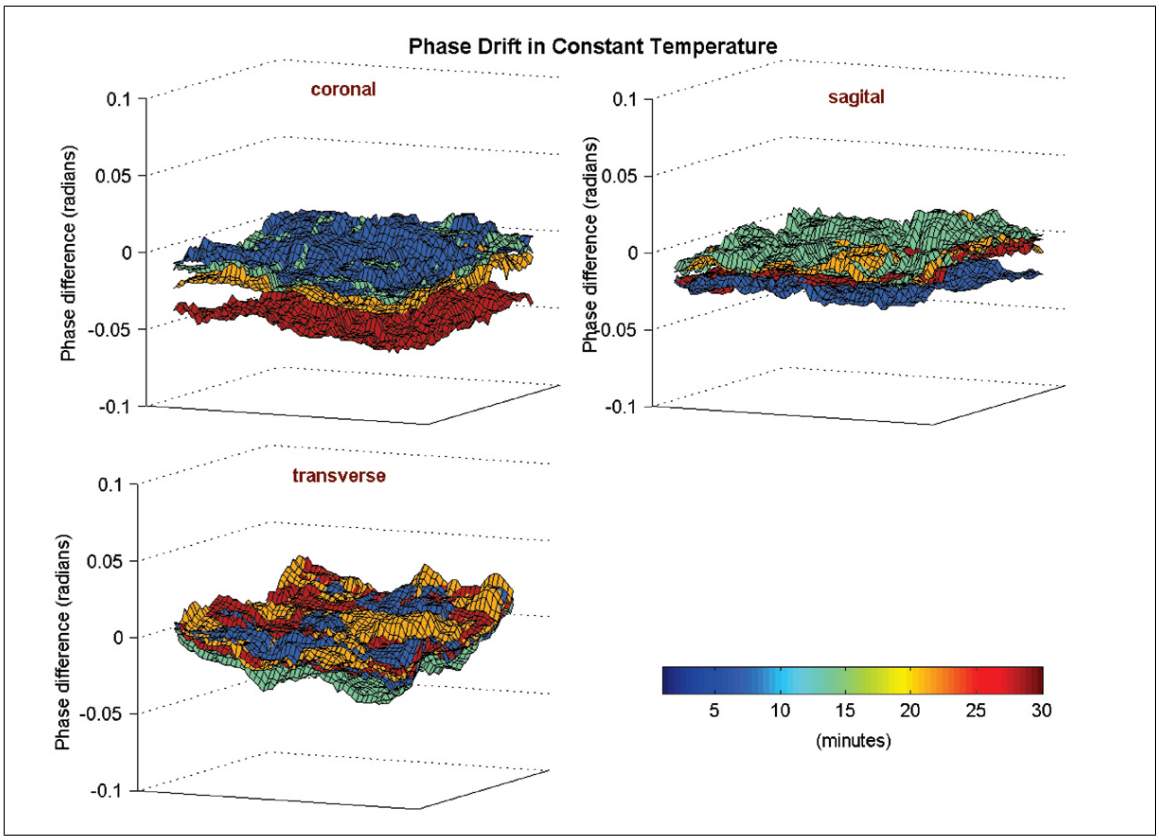

Figure 4.2 Phase drift at constant room temperature

Planar nature of the phase drift can be observed in all three perpendicular planes, although transverse plane contains more distortion than the others. This set was chosen for further analysis since it is subject to the greatest amount of drift.

4.2 Correction algorithm

For validation of the correction scheme, 1 region of analysis in the center and 4 regions of reference in the corners were selected (Figures 4.3 and 4.4).

Best fit planes were estimated for each time frame using a minimum euclidean distance algorithm, and only the data in the four regions of reference were used for the extraction of these planes. Reference planes were subtracted from each frame

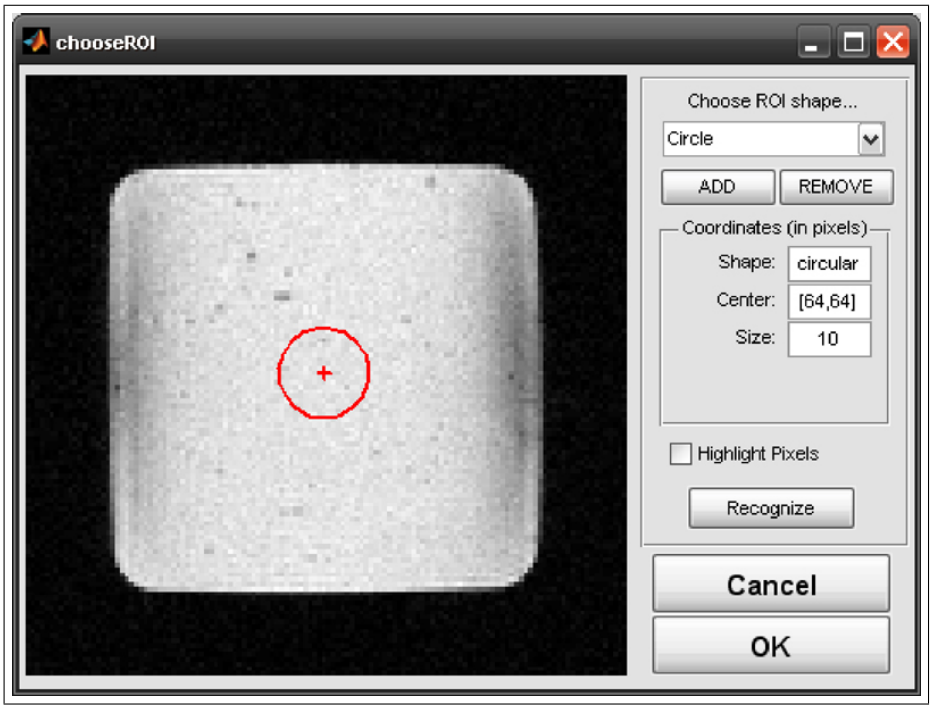

Figure 4.3 Region of analysis for phase drift correction

to obtain drift corrected phase difference images. Raw and drift corrected sets are then mapped to temperature difference. Figure 4.5 plots the temperature difference averaged the circular region of analysis. The phantom was placed in the exam room two hours prior to the shooting to make sure it reaches thermal equilibrium. And since it was completely enclosed in styrofoam, we can assume the phantom was in constant temperature for the purposes of this exam. Thus $\Delta T = 0$ line can be assumed to be the actual value.

Phase difference is hardware related and its nature and magnitude is highly unpredictable. In this case it was restricted to below 0.05 *radians* over 30 minutes, which corresponds to a perceived increase of 1 $^{\circ}C$ in temperature. The method we used was found to be successful to correct, bringing even this small amount of deviation back to the baseline. Our temperature mapping experiment turned out to be subjected to a greater amount of drift, and the results of the drift correction on that data can be seen in figure 5.2.

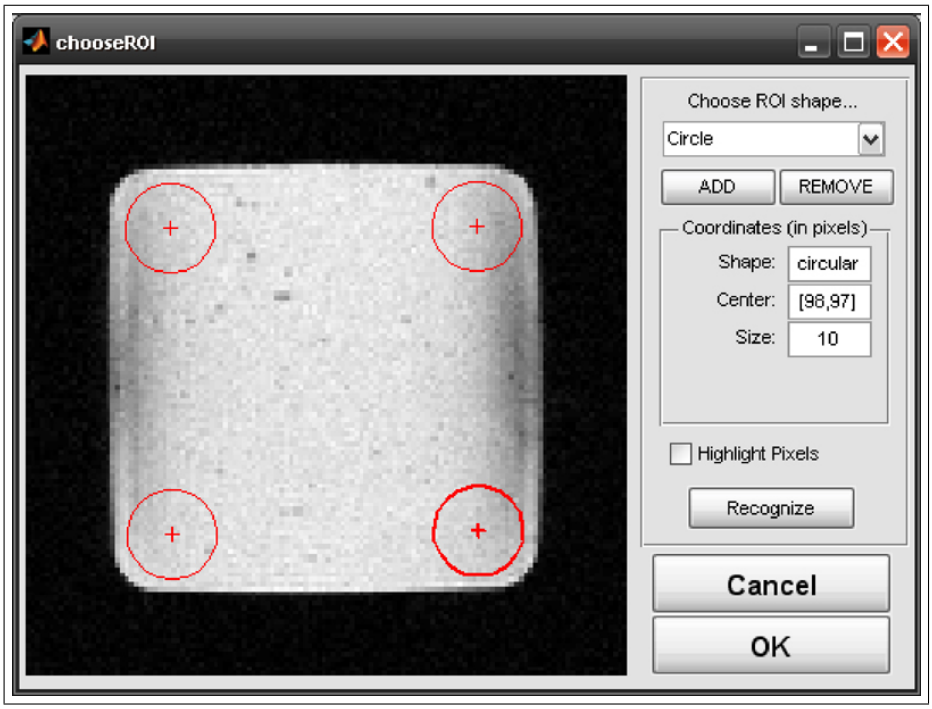

Figure 4.4 Regions of reference for phase drift correction

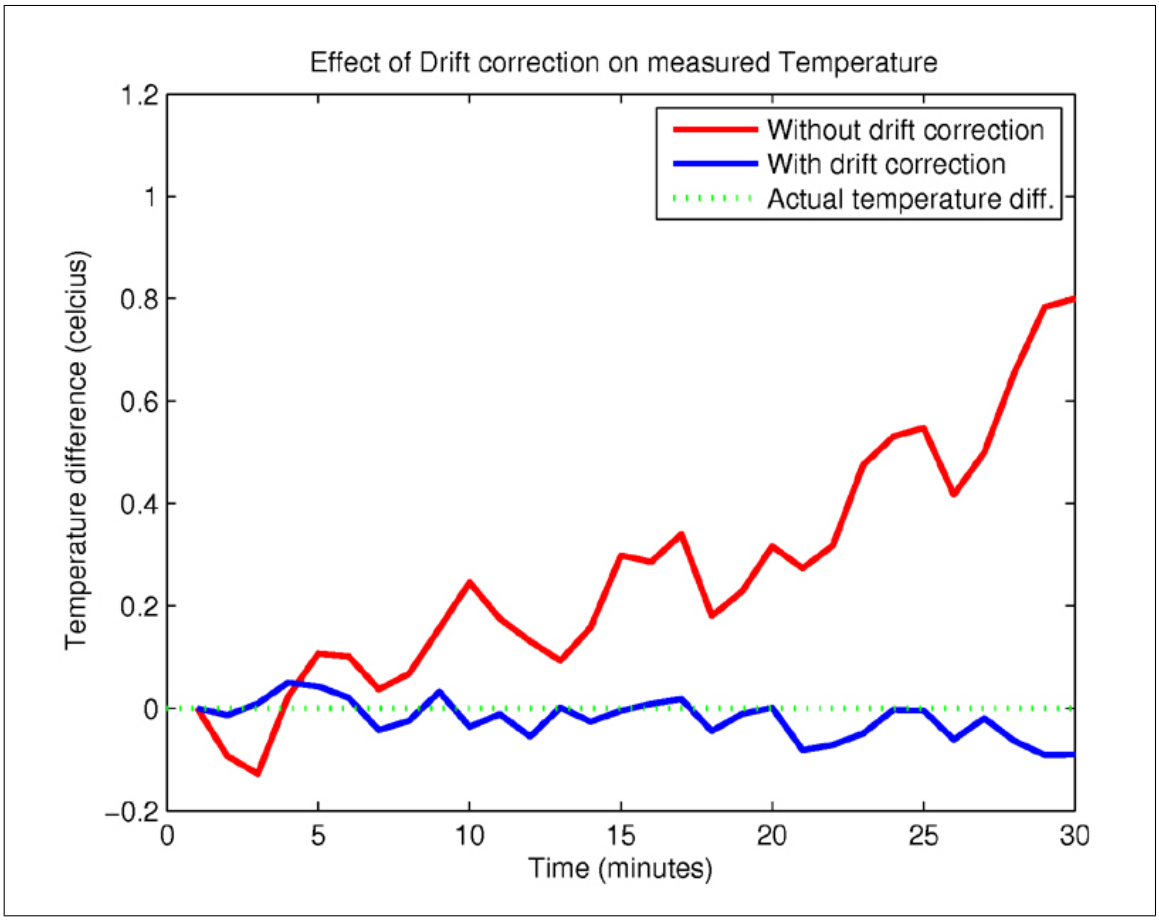

Figure 4.5 Effect of drift correction on measured temperature

5. TEMPERATURE MEASUREMENT WITH GRADIENT ECHO

The setup described in sections 3.2 and 3.3 were placed in the head coil of a $1.5T$ MRI scanner. GRE phase images (seq.: FLASH, $TE/TR = 15/29$, $\alpha = 30°$) were acquired every thirty seconds during a heating period of 15 minutes and a passive cooling of 20 mins. Ishihara's method described in section 2.3.3 is used to extract thermal distribution from the successive phase images.

Phase drift correction algorithm was also applied to the resulting thermal distribution data, as outlined in section 4, using the reference data at locations presented in figure 5.1.

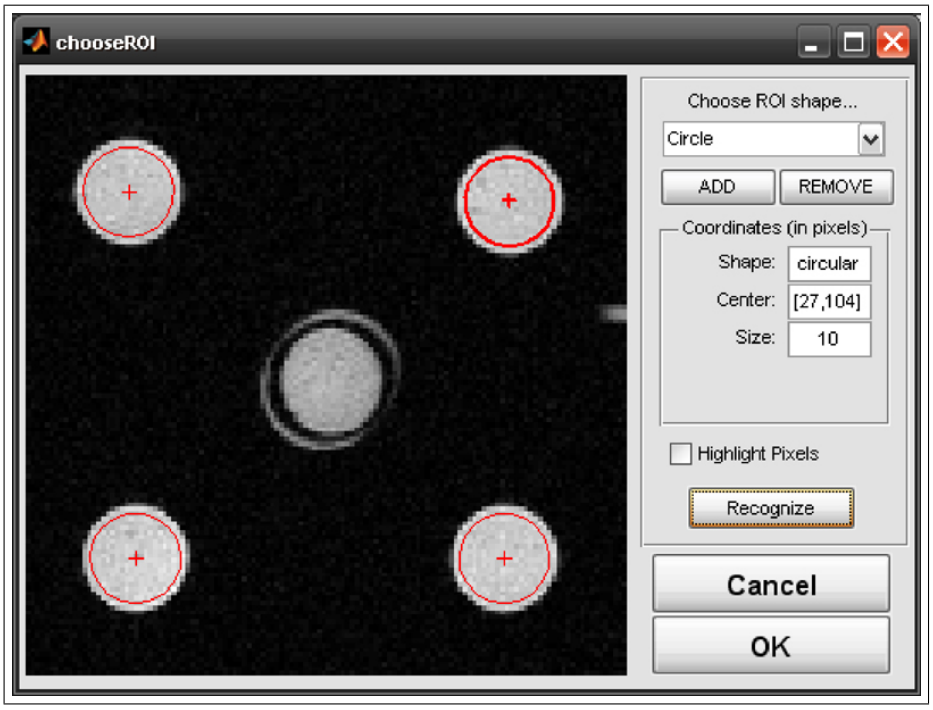

Figure 5.1 Regions of reference for drift correction

Region of analysis is also circular, and is center coincides with the center of the tube phantom in the middle. Average temperature of different size regions are plotted in figure 5.2 for demonstration.

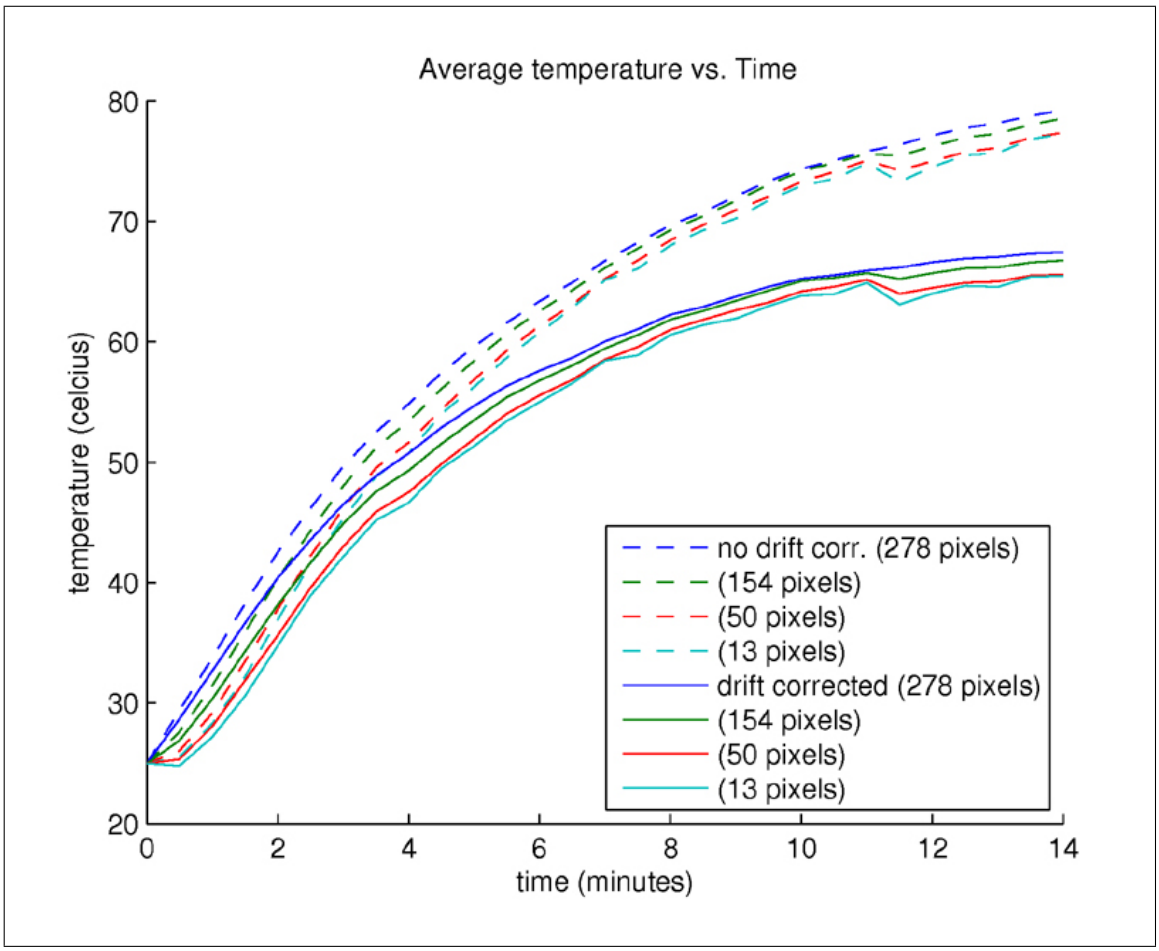

Figure 5.2 Average Temperature vs. Time, over concentric circular regions.

As one can see, the curves vary both in smoothness and trend, as expected. Heating system used in this experiment is strong enough to create a temperature gradient over the cross section of the tube. Until the system reaches thermal equilibrium (which does not yet happen in this graph, pixels close to the center will be cooler. Smaller of the concentric regions reflect this perfectly on figure 5.2.

Since a temperature gradient is present, it is better to visualize it using thermal maps. A thermal map was created from the temperature distribution data, by assigning temperature ranges to different colors. Figure 5.3 and 5.3 contain snapshots of this thermal map at different times.

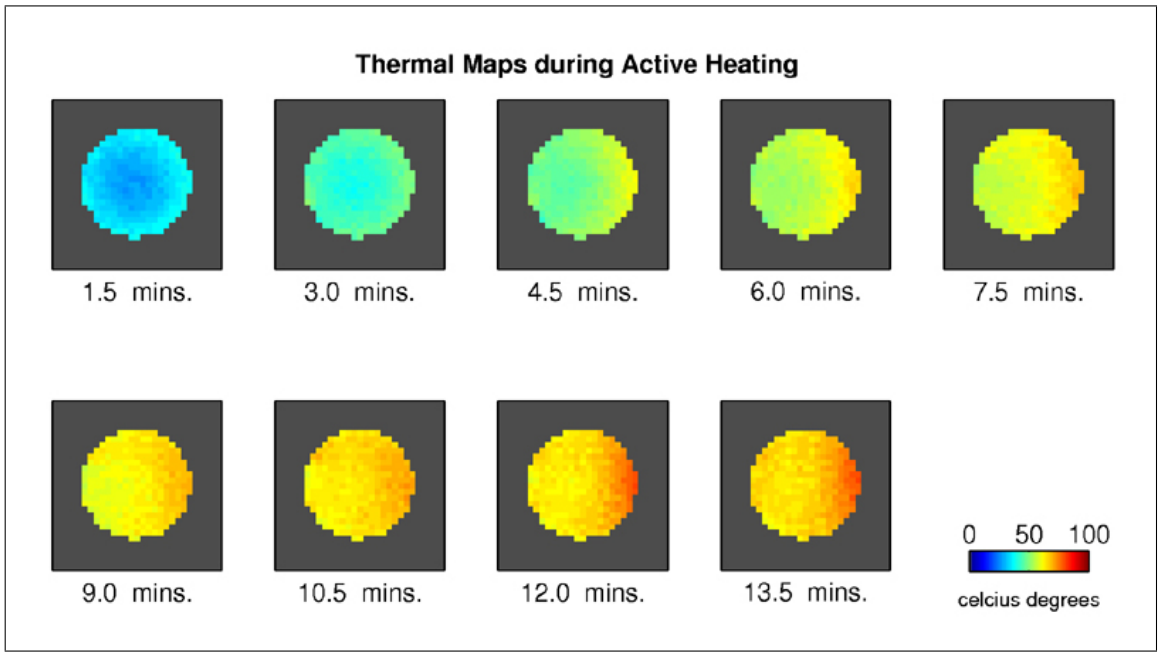

Figure 5.3 Thermal Map snapshots during active heating

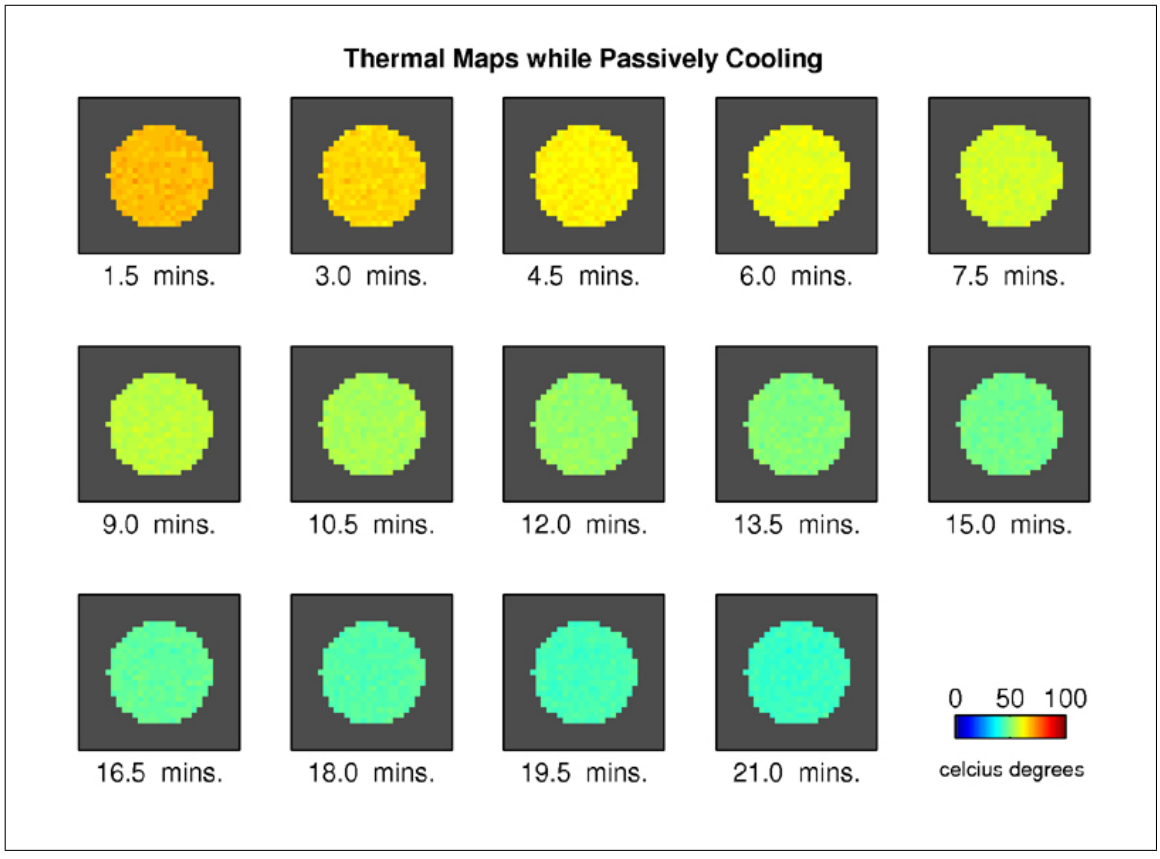

Figure 5.4 Thermal Map snapshots during cooling

6. EFFECT OF ECHO TIME ON THERMAL RESOLUTION

The theoretical SNR of temperature measurement with GRE maximizes when $TE = T_2^*$ [20]. Therefore choice of proper sequence parameters is not as straightforward as maximizing the SNR of the received magnitude image. In this study, we investigated the effect of different echo times on temperature measurement by spanning a range of TE between 5 and $40ms$. For comparison purposes, TR was fixed to $50ms$ even though this is unnecessarily large for some of the TE values.

The setup for phase drift correction in chapter 5 was also used for this study. Otherwise identical sequences with $TE = \{5, 10, 20, 30, 40\}ms$ were run in a loop for 30 minutes. Pauses between each shot are arranged so that two consecutive identical sequences were executed with 30 second intervals. Analysis is constrained to the four reference phantoms in the corners (figure 6.1), which maintain a constant temperature. Phase images were processed in the way described in chapter 5, until temperature distribution matrices are obtained for each different TE value.

Since this approach produces only relative measurements, we used variance of temperature difference time series, which are inversely proportional to SNR of the system. Variance of the time series was calculated for each pixel, then averaged over the pixels the regions of interest. Results are summarized in figure 6.2.

The graph suggests a minimum point around $TE = 30$. According to Quesson's derived SNR equation, SNR beyond the minimum point is relatively flat, thus our current range of ($5ms <= TE <= 40ms$) should be sufficient to conclude that $T_2^* \approx 30ms$ for our gel phantom, and also the thermal resolution of our system can get as low as 0.2 $^\circ C$. However, that would require a larger TR. Parameters for the evaluation of the system were tuned to $TE/TR = 15/29$ to restrain acquisition time to under $4s$ for a $128x128$ matrix size. With these restrictions, figure 6.2 suggests that our thermal resolution is around 0.5 $^\circ C$.

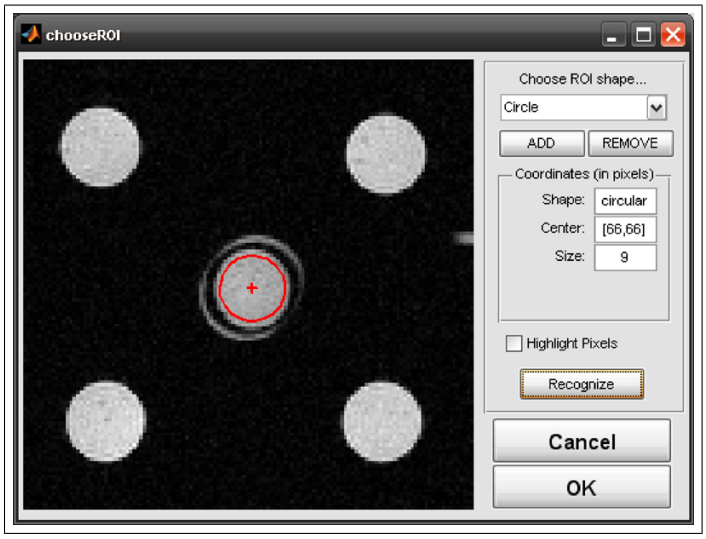

Figure 6.1 Region of analysis for TE effect on thermal resolution

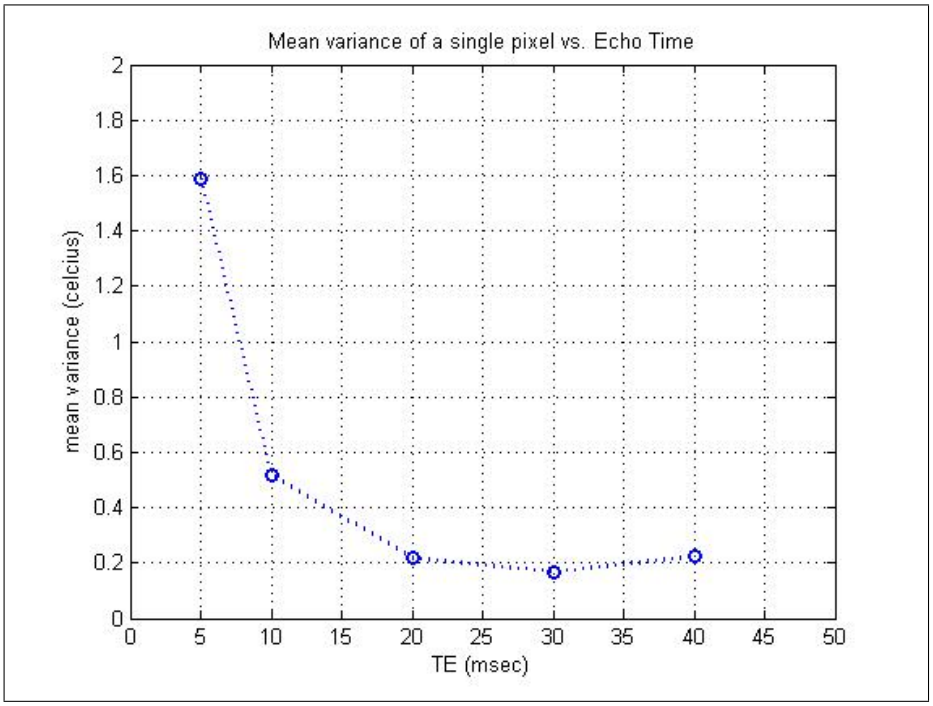

Figure 6.2 Mean variance of temperature difference measured at a single pixel vs. Echo time; under constant phantom temperature

7. CONCLUSION

Three main studies were performed during the course of this thesis. First one is the investigation of the phase drift phenomenon and evaluation of a corrective algorithm. It was observed that the assumption of a planar drift holds in all perpendicular planes, and constant temperature reference phantoms can be used to estimate and compensate for this deviation. It is particularly noteworthy that if relatively large areas for reference are available, even the slightest amount of drift with the same order of magnitude with the apparent noise in the system, can be corrected.

It is also observed that phase drift varies greatly among different setups. Drift amount in our heating experiment was several orders of magnitude larger that the one in the constant temperature trial. This phase drift is a result of many phenomenon such as hardware calibration and shimming procedure. Even the workload of the scanner prior to the experiment may have an effect. This unpredictable nature of phase drift is yet another indication to its necessity.

It is reported that the SNR of thermal imaging through phase difference images attains it's maximum at $TE = T_2^*$. Our parameter spanning experiment demonstrated this behavior with mean variance of measured temperature reaching its minimum at $TE = 30ms$. This study also shows the practical limit of the thermal resolution with the current system, which is measured to be 0.2 $^\circ C$.

In the main study of this thesis, we were able to obtain thermal maps of our gel phantom. Our system is capable of creating near real–time thermal maps for a $128x128$ matrix with a spatial resolution of $0.8cm$. Our temporal resolution is roughly 4 seconds, and our thermal resolution is measured to be 0.4 $^\circ C$. It should be noted that temporal and thermal resolution can be traded off to obtain more accurate thermal maps or faster acquisitions.

For a true quantitative analysis and verification, transducers such as fiber optic probes need to be used simultaneously, which is not possible with our current setup. However, there is an abundance of such published studies in the recent years, and MRTI with GRE sequence is on the path to becoming a golden standard. Our initial goal was to use this approach to put together pieces of tools which is capable of performing real time temperature measurement, is met.

REFERENCES

1. Falk, M. H., and R. D. Issels, "Hyperthermia in oncology," *Int. J. Hperthermia*, Vol. 17, no. 1, pp. 1–18, 2001.

2. Gonzalez, D. G., J. D. P. V. Dijk, L. E. C. M. Blank, and P. Rümke, "Combined Treatment with Radiation and Hyperthermia in Metastatic Malignant Melanoma," *Radiotherapy in Oncology*, Vol. 6, pp. 105–113, 1986.

3. Hou, B. S., Q. B. Xiong, and D. J. Li, "Thermo-chemo-radiotherapy of Esophageal Cancer, A Preliminary Report on 34 Cases," *Cancer*, Vol. 64, pp. 1777–1782, 1989.

4. Ueo, H., and K. Sugimachi, "Preoperative Hyperthermochemoradiotherapy for Patients with Esophageal Carcinoma or Rectal Carcinoma," *Seminars in Surgical Oncology*, Vol. 6, pp. 8–13, 1990.

5. Zee, J. V. D., D. G. Gonzalez, C. G. V. Rhoon, J. D. V. Dijk, W. L. Putten, and A. A. Hart, "Comparison of Radiotherapy Alone with Radiotherapy plus Hyperthermia in Locally Advanced Pelvic Tumours: A Prospective, Randomised, Multicentre Trial," *The Lancet,*, Vol. 355, pp. 1119–1125, 2000.

6. Kacher, D. F., and F. A. Jolesz, "MR Imaging Guided Breast Ablative Therapy," *Radiol Clin N Am*, Vol. 42, pp. 947–962, 2004.

7. Boetes, C., R. D. Mus, R. Holland, J. O. Barentsz, S. P. Strijk, and T. W. and, "Breast Tumours: Comparative Accuracy of MR Imaging Relative to Mammography and US for Demonstrating Extent.," *Radiology*, Vol. 197, pp. 743–747, 1995.

8. Bleier, A. R., F. A. Jolesz, M. S. Cohen, R. M. Weisskoff, J. J. Dalcanton, and N. H. and, "Real-time Magnetic Resonance Imaging of Laser Heat Deposition in Tissue," *Magn Reson Med*, Vol. 21, pp. 132–137, 1991.

9. Lai, L. M., M. A. Hall-Craggs, H. Mumtaz, P. M. Ripley, and M. K. and, "Interstitial Laser Photocoagulation for Fibroadenomas of the Breast," *Breast*, Vol. 8, pp. 89–94, 1999.

10. Harms, S., H. Mumtaz, T. Hronas, C. Cowan, S. Khmberg, and B. a. Hyslop, "MRI Directed Interstitial Thermal Ablation of Breast Fibroadenomas," in *Seventh Proceedings of the International Society of Magnetic Resonance Medicine, Hoboken (NJ)*, Wiley & Sons, Inc., 1999.

11. Cline, H. E., K. Hynynen, R. D. Watkins, W. J. Adams, J. F. Schenck, and R. H. Ettinger, "A focused ultrasound system for MRI-guided ablation.," *Radiology*, Vol. 194, pp. 731–737, 1995.

12. McDannold, N., K. Hynynen, and F. Jolesz, "MRI Monitoring of the Thermal Ablation of Tissue: Effects of Long Exposure Times," *J Magn Reson Imaging*, Vol. 13, pp. 421–427, 2001.

13. Cline, H., J. Schenck, R. Watkins, K. Hynynen, and F. Jolesz, "Magnetic Resonance-Guided Thermal Surgery," *Magn Reson Med*, Vol. 30, pp. 98–106, 1993.

14. McDannold, N., K. Hynynen, D. Wolf, G. Wolf, and F. Jolesz, "MRI Evaluation of Thermal Ablation of Tumors with Focused Ultrasound," *J Magn Reson Imaging*, Vol. 8, pp. 91–100, 1998.

15. Fenn, A., G. Wolf, and R. Fogle, "An Adaptive Microwave Phased Array for Targeted Heating of Deep Tumours in Intact Breast: Animal Study Results," *Int J Hyperthermia*, Vol. 15, pp. 45–61, 1999.

16. Wansapura, J., B. Daniel, J. Pauly, and K. Butts, "Temperature Mapping of Frozen Tissue Using Eddy Current Compensated Half Excitation RF Pulses," *Magn Reson Med*, Vol. 46, pp. 985–992, 2001.

17. Fallone, B., P. Moran, and E. Podgorsak, "Noninvasive Thermometry with a Clinical X-Ray CT Scanner," *Medical Physics*, Vol. 9, pp. 715–721, 1982.

18. Pernot, M., M. Tanter, J. Bercoff, K. R. Waters, and M. Fink, "Temperature Estimation Using Ultrasonic Spatial Compound Imaging," *IEEE Transactions on Ultrasonics, Ferroelectrics, and Frequency Control*, Vol. 51, pp. 606–615, May 2004.

19. Senneville, B. D. D., B. Quesson, and C. T. W. Moonen, "Magnetic Resonance Temperature Imaging," *Int. J. Hyperthermia*, Vol. 21, pp. 515–531, September 2005.

20. Quesson, B., J. A. de Zwart, and C. T. Moonen, "Magnetic Resonance Temperature Imaging for Guidance of Thermotherapy," *Journal of Magnetic Resonance Imaging*, Vol. 12, pp. 525–533, 2000.

21. Botnar, R., "Temperature Sensitive MR Sequences," in *Interventional Magnetic Resonance Imaging*, 1998.

22. Nekolla, S., T. Gneiting, J. Syha, R. Deichmann, and A. Haase, "T1 Maps by K-space Reduced Snapshot-FLASH MRI," *J Comput Assist Tomogr*, Vol. 16, pp. 327–332, 1992.

23. Crawley, A., and R. Henkelman, "A Comparison of One-Shot and Recovery Methods in T1 Imaging," *Magn Reson Med*, Vol. 7, pp. 23–34, 1998.

24. Matsumoto, R., R. Mulkern, S. Hushek, and F. Jolesz, "Tissue Temperature Monitoring for Thermal Interventional Therapy: Comparison of T1-weighted MR Sequences," *J Magn Reson Imaging*, Vol. 4, pp. 65–70, 1994.

25. Wlodarczyk, W., M. Hentschel, P. Wust, R. Noeskek, N. Hosten, H. Rinnebergk, and R. Felix, "Comparison of four magnetic resonance methods for mapping small temperature changes," *Phys. Med. Biol.*, Vol. 44, pp. 607–624, 1999.

26. Graham, S., G. Stanisz, A. Kecojevic, M. Bronskill, and R. Henkelman, "Analysis of Changes in MR Properties of Tissues After Heat Treatment," *Magnetic Resonance in Medicine 42:1061-1071 (1999)*, Vol. 42, pp. 1061–1071, 1999.

27. Fried, M., P. Morrison, S. Hushek, G. Kernahan, and F. Jolesz, "Dynamic T1-Weighted Magnetic Resonance Imaging of Interstitial Laser Photocoagulation in the Liver: Observations on in vivo Temperature Sensitivity," *Lasers Surg Med*, Vol. 18, pp. 410–419, 1996.

28. Hynynen, K., N. McDannold, R. V. Mulkern, and F. A. Jolesz, "Temperature Monitoring in Fat With MRI," *Magnetic Resonance in Medicine*, Vol. 43, pp. 901–904, 2000.

29. Schneider, W. G., H. J. Bernstein, and J. A. Pople, "Proton Magnetic Resonance Chemical Shift of Free (Gaseous) and Associated (Liquid) Hydride Molecules," *J. Chem. Phys. 28*, Vol. 28, pp. 601–607, 1958.

30. Muller, N., and R. C. Reiter, "Temperature Dependence of Chemical Shifts of Protons in Hydrogen Bonds," *J. Chem. Phys*, Vol. 42, pp. 3265–3269, 1965.

31. Muller, N., "Concerning Structural Models for Water and Chemical-Shift Data," *J. Chem. Phys*, Vol. 43, pp. 2555–2556, 1965.

32. Hindman, J. C., "Proton Resonance Shift of Water in the Gas and Liquid States," *The Journal of Chemical Physics*, Vol. 44, no. 12, pp. 4582–4592, 1966.

33. Ishihara, Y., A. Calderon, and H. a. Watanabe, "A Precise and Fast Temperature Mapping Method Using Water Proton Chemical Shift," in *Proceedings of the SMRM Annual Meeting, Berlin*, p. 4803, 1992.

34. Ishihara, Y., A. Calderon, H. Watanabe, K. Okamato, Y. Suzuki, K. Kuroda, and Y. Suzuki, "A Precise and Fast Temperature Mapping Using Water Proton Chemical Shift," *Magnetic Resonance in Medicine*, Vol. 34, pp. 814–823, 1995.

35. Hornak, J., *The Basics of MRI*, www.cis.rit.edu/htbooks/mri/, 1996.

36. Poorter, J. D., C. D. Wagter, and J. Maier, "The Proton Resonance Frequency Shift Method Compared with Molecular Diffusion for Quantitative Measurements of Two-Dimensional Time Dependent Temperature Distributions in a Phantom," *J. Magn. Reson.*, Vol. 103, pp. 234–241, 1994.

37. Poorter, J. D., C. D. Wagter, Y. D. Deene, C. Thomsen, F. Stahlberg, and E. Achten, "Noninvasive MRI Thermometry with the Proton Resonance Frequency (PRF) Method: In Vivo Results in Human Muscle," *Magnetic Resonance in Medicine 33 74-81 1995*, Vol. 33, pp. 74–81, 1995.

38. Senneville, B. D. D., P. Desbarats, B. Quesson, and C. T. W. Moonen, "Real-Time Artefact Corrections For Quantitative MR Temperature Mapping," *Journal of WSCG*, Vol. 11, February 2003.

39. Senneville, B. D. D., B. Quesson, F. Desbarats, R. Salomir, J. Palussiere, and C. T. W. Moonen, "Atlas-Based Motion Correction for On-Line MR Temperature Mapping," in *International Conference on Image Processing (ICIP)*, 2004.

40. Vigen, K. K., B. L. Daniel, J. M. Pauly, and K. Butts, "Triggered, Navigated, Multi-Baseline Method for Proton Resonance Frequency Temperature Mapping With Respiratory Motion," *Magnetic Resonance in Medicine*, Vol. 50, pp. 1003–1010, 2003.

41. Zwart, J. A. D., F. C. Vimeux, J. Palussiere, R. Salomir, B. Quesson, C. Delalande, and C. T. Moonen1, "On-Line Correction and Visualization of Motion During MRI-Controlled Hyperthermia," *Magnetic Resonance in Medicine*, Vol. 45, pp. 128–137, 2001.

42. Kuroda, K., R. Mulkern, K. Oshio, L. P. Panych, T. Nakai, T. Moriya, S. Okuda, K. Hynynen, and F. Joles, "Temperature Mapping Using the Water Proton Chemical Shift: Self-Referenced Method With Echo-Planar Spectroscopic Imaging," *Magnetic Resonance in Medicine*, Vol. 43, pp. 220–225, 2000.

43. Rieke, V., A. B. Ross, W. H. Nau, C. J. Diederich, G. Sommer, and K. Butts, "MRI-temperature mapping during ultrasound prostate ablation using fat for phase estimation," in *Proceedings of the 26th Annual International Conference of the IEEE EMBS*, (San Francisco, CA, USA), September 2004.

44. Rieke, V., K. K. Vigen, G. Sommer, B. L. Daniel, J. M. Pauly, and K. Butts, "Referenceless PRF Shift Thermometry," *Magnetic Resonance in Medicine*, Vol. 51, pp. 1223–1231, 2004.

45. Boss, A., H. Graf, B. Muller-Bierl, S. Clasen, D. Schmidt, P. L. Pereira, and F. Schick, "Magnetic Susceptibility Effects on the Accuracy of MR Temperature Monitoring by the Proton Resonance Frequency Method," *Journal Of Magnetic Resonance Imaging*, Vol. 22, pp. 813–820, 2005.

46. Shmatukha, A. V., and C. J. G. Bakker, "Correction of proton resonance frequency shift temperature maps for magnetic field disturbances caused by breathing," *Phys. Med. Biol.*, Vol. 51, pp. 4689–4705, 2006.

47. Tempany, C. M. C., E. A. Stewart, N. McDannold, B. J. Quade, F. A. Jolesz, and K. Hynynen, "MR Imaging-guided Focused Ultrasound Surgery of Uterine Leiomyomas: A Feasibility Study," *Radiology*, Vol. 226, p. 897905, 2003.

48. Hesley, G. K., J. P. Felmlee, J. B. Gebhart, K. T. Dunagan, K. R. Gorny, J. B. Kesler, K. R. Brandt, J. N. Glantz, and B. S. Gostout, "Noninvasive Treatment of Uterine Fibroids: Early Mayo Clinic Experience With Magnetic Resonance Imaging-Guided Focused Ultrasound," *Mayo Clin Proc.*, Vol. 81, pp. 936–942, 2006.

49. Pilatou, M. C., E. A. Stewart, S. E. Maier, F. Fennessy, K. Hynynen, C. M. Tempany, and N. McDannold, "MR Temperature Mapping and Diffusion-weighted Imaging of Focused Ultrasound Surgery of Uterine Fibroids: Preliminary," in *Proc. Intl. Soc. Mag. Reson. Med.*, 2007.

50. McDannold, N., M. Moss, R. Killiany, D. L. Rosene, . Randy L. King Ferenc A. Jolesz, and K. Hynynen1, "Mri-guided focused ultrasound surgery in the brain: Tests in a primate model." online, 2003.

51. Stafford, R. J., J. S. Weinberg, R. J. McNichols, A. Gowda, A. Shetty, A. M. Elliott, A. Borne, R. Uthamanthil, and J. D. Hazle, "MR-guided Laser Induced Thermal Therapy in Normal Canine Brain: Pre-clinical Device Evaluation," in *Proc. Intl. Soc. Mag. Reson. Med.*, 2007.

52. Chopra, R., N. Baker, V. Choy, A. Boyes, K. Tang, S. Appu, L. Klotz2, and M. Bronskill, "Targeted treatment of localized regions within the prostate gland using MRI-guided transurethral ultrasound therapy," in *Proc. Intl. Soc. Mag. Reson. Med.*, 2007.

53. Kinoshita, M., N. McDannold, F. A. Jolesz, and K. Hynynen, "Noninvasive localized delivery of herceptin to the mouse brain by mri-guided focused ultrasound-induced blood-brain barrier disruption." online, 2006.

54. Kinoshita, M., N. McDannold, F. A. Jolesz, and K. Hynynen, "Targeted delivery of antibodies through the blood-brain barrier by MRI-guided focused ultrasound," *Biochemical and Biophysical Research Communications*, Vol. 340, pp. 1085–1090, 2006.

55. Quesson, B., and C. T. W. Moonen, "Spatial and temporal control of transgene expression using MRI-guided Focused Ultrasound," *Medicamundi*, Vol. 47, pp. 48–56, 2003.